4-10-4

FEASIBILITY STUDY FOR THE DESIGN OF A PORTABLE ROCK/COAL DUST METER

by

HARBANS BEHARI MATHUR

Submitted in Partial Fulfillment of the Requirement
for the Degree of
Master of Science
in the
Electrical Engineering
Program

Salvatore R. Pansino 3/2/90

Advisor Date

Sally M. Hotchkiss March 8 1990

Dean of the Graduate School Date

YOUNGSTOWN STATE UNIVERSITY

MARCH , 1990

ABSTRACT

FEASIBILITY STUDY FOR THE DESIGN OF A PORTABLE ROCK/COAL DUST METER

Harbans Behari Mathur

Master of Science, Electrical Engineering

Youngstown State University, 1990

This thesis deals with a feasibility study for the design of a Rock/Coal Dust Meter (RD meter) using an optical fiber probe, i.e., to investigate and develop a method to determine the safe percentage (by weight) of Rock Dust (RD) in a mixture of Coal Dust and Rock Dust sample. The goal is to develop a model that will predict the results of laboratory experiments. This model will be used to determine the feasibility of developing a RD meter, and to investigate the relationship of existing theory to laboratory measurements.

The attenuation, reflection and scattering of light waves from a coal/rock dust surface are important elements in such investigations. Currently, a large amount of research and development work is being done by researchers in other fields, e.g., the determination of the oxygen content in blood by measuring the diffuse reflectance. Such an RD meter may be used to detect dangerous levels of coal dust in coal mines; coal mine explosions may then be averted .

ACKNOWLEDGEMENTS

My sincere gratitude is extended to Dr.Salvatore R. Pansino, Professor and Chairman of the Department of Electrical Engineering, Y.S.U., and also to Dr. Henry Perlee, United States Bureau of Mines, Pittsburgh, Pennsylvania, for their valued advice and guidance throughout the thesis.

I would also like to thank Dr.Duane F. Rost, Professor of Electrical Engineering and Chairman of my student advisory committee, Y.S.U., for his encouragement.

Special thanks is also extended to Dr. Gus Mavrigian, Professor, Mathematics Department, YSU for his assistance in the understanding of the higher mathematics involved in the development of the theory for this project.

Thanks also to Dr. Dilip Singh, Chairman, Chemical Engineering Department, YSU for providing the Fiber Optic kit for this investigation. Help also came from other sources and is acknowledged, appropriately, throughout the report.

Finally, my sincere and loving thanks to my wife Suman for her encouragement, understanding, and support throughout my course of advanced study, here at Youngstown State University.

TABLE OF CONTENTS

LIST OF SYMBOLS

SYMBOL	DEFINITION	UNITS
CD	Coal Dust	
OFP	Optical Fiber Probe	
OF	Optical Fiber	
OP-AMP	Operational Amplifier	
RD	Rock Dust	
Å	Angstrom Unit	(1 Å = 10^{-10} meters)
c	Velocity of light in vacuum	($\approx 3\times10^{8}$ m/s)
e	Exponential Constant	(=2.718)
eV	Electron volts	(1 eV = 1.60 × 10^{-19} Joules)
f	Frequency	Hertz
h	Planck's constant	(=6.626 × 10^{-34} Joules.s or 4.141 × 10^{-15} eV.s)
k	Wave Number	(= $2\pi/\lambda$) m^{-1}
ln	Natural Log	
m	Length	meters
n	Refractive index of a medium	
s	Time	seconds
v	Velocity of light in a medium	m/s
N.A.	Numerical aperture of an optical fiber	
α_r	Reflectivity coefficient	
α_s	Scatter coefficient	
α_t	Total absorption coefficient	$\alpha_t = \alpha_r + \alpha_s$
ε	Permittivity of a medium	($\varepsilon = \varepsilon_r \times \varepsilon_o$) F/m

SYMBOL	DEFINITION	UNITS
ϵ_o	Vacuum permittivity	$(= 8.854 \times 10^{-12})$ F/m
ϵ_r	Relative permittivity of a medium	
λ	Wavelength	(v/f) meters
μ_o	Vacuum permeability	$(= 4\pi \times 10^{-7})$ H/m
μ	Permeability of a medium	H/m
π	A geometrical constant	(= 3.14159)
θ	Angle	degrees
θ_1	Angle of incidence	degrees
θ_1'	Angle of reflection	degrees
θ_2	Angle of refraction	degrees
θ_c	Critical angle	degrees

LIST OF FIGURES

LIST OF TABLES

CHAPTER I

INTRODUCTION

1.1 OBJECTIVE

The objective of this project is to conduct a feasibility study for the design of a portable battery-powered RD meter capable of distinguishing between safe and unsafe Coal Dust - Rock Dust mixtures. The experiments conducted indicate that the change in reflectance property of the sample with concentration of RD (using an infrared or near infrared light source).

The following tasks are set in order to accomplish this objective.

1. Understand optical fibers and their application as a probe.
2. Design a suitable electronic circuit to measure light backscatter/reflectance in terms of electrical parameters.
3. Measure Coal and Rock Dust light reflectance.

1.2 BACKGROUND

Many years of research on explosion by the United States Bureau of Mines, and similar agencies in other countries have shown that mixing a specific/critical quantity of inert dust (Rock Dust) with Coal Dust (CD) will prevent Coal Dust explosions. Rock dusting is required by Federal Code in underground coal mines in the United States with limestone dust, the most commonly used substance. The law requires 80 wt pct incombustible material in the dust deposited in returns and 65 wt pct elsewhere in the mine, except for the first 40 ft (12.2 meters) from the face, where only crosscuts must be rock dusted[1].

In the presence of methane, the incombustible content of the dust must be increased by 0.4 pct in returns and 1 pct elsewhere, for each 0.1 wt pct methane in the ventilating air. An inspector for the Mine Safety & Health Administration (MSHA), in compliance with the law, periodically collects the samples of deposited dust.

The conventional sample comes from a 6 inch (152.4mm) wide band across the floor, ribs and roof to a depth of 1 inch (25.4 mm) , where possible. If the floor is well rock dusted, but the roof and ribs are determined visually to be deficient in Rock Dust content, then it is recommended that the combined rib and roof portion of the band sample be kept separate from the floor portion, and a separate analysis be made on each. The inspector screens the sample through a No. 10 sieve, if possible, and sends about 200 gms of the sieved sample to the laboratory for analysis.

The concentration of Rock Dust in the sample is

NOTE: Superscript numbers throughout the thesis correspond to numbers in the bibliography.

obtained by volumetric methods. From this Rock Dust measurement, the incombustible content is computed. Typically, the results of the analysis are received about two weeks after the sample is taken. In the mean time, the mine operators must rely on visual inspection (grayness) of rock dusted areas to estimate the quality of the rock dusting practice on a daily basis.

For the past few years the Bureau of Mines has been developing several radiometric meters to measure Rock Dust in dust samples to help reduce the time delay and expense involved in the analysis. Meters utilizing beta (β) and gamma (γ) radiation have been built; the β and γ-rays were noted to react strongly with Ca (Calcium) and Mg (Magnesium) atoms present in the Rock Dust and ash, but react weakly with H (Hydrogen), C (Carbon) or O (Oxygen) atoms found in the coal or water. To date, such single energy level radiometric approaches for measuring the rock dust and ash content of mine dust samples (excluding water) are limited to large samples and non-portable equipment[2].

To alleviate the problems cited above, the Bureau of Mines designed and constructed a portable optical RD meter, that measures the concentration of RD in a primary RD/CD mixture (measuring the dust's optical reflectivity). The task performed by their portable meter provides a simple and rapid determination of the Rock Dust content in the grab samples[2].

The Bureau of Mine's optical Rock Dust probe has several drawbacks, namely[2]:

a) sensitivity to moisture
b) dust compaction, and
c) particle size distribution.

The purpose of their research was to determine if spatial distribution and polarization of photons, scattered from a dust layer, aids in the building of a meter that is not sensitive to above three factors. In the first phase of their research, they concentrated on studying the spatial distribution of the scattered photons, leaving the polarization studies for possible future research.

Much optical backscatter work has been done by researchers in the bio-medical field for the design of meters to measure oxygen concentration in blood[3,4,5,6,8,9,10].

1.3 BUREAU OF MINES RD METER

The Bureau of Mines RD meter is capable of measuring the Rock Dust concentrations of samples and therefore total incombustible content, giving the ash and water percentage, either in a mine's office or by taking direct measurements in underground roadways (tunnels). The operation of the meter is based on the measurement of infrared light reflected from the sample surface, consisting of a mixture of dark CD and light RD particles. Their RD meter measurements indicate that the amount of light reflected from the sample surface increases with an increase in the concentration of RD in the sample[2]. The correlation obtained with prepared dust samples is within ±2% of results determined by chemical analysis for Rock Dust contents with 30 to 100 weight pct. The response of their meter has been most encouraging, and if further testing confirms its reliability, industry will have means of making rock dusting more effective, thus increasing safety and lowering the cost of chemical analysis.

CHAPTER 2

THEORY

2.1 INTRODUCTION

The transport of photons in a dust layer include three stochastic processes: (a) the travel of the photon in the void (air filled) spaces between the particles, (b) the absorption of the photons by the particles, and (c) the scattering of the photons by the particles.

Each of the above processes is characterized by a single parameter: (a) the parameter centers on the particle mean-free path ($\bar{l}$); (b) it is the absorption coefficient (α); and in (c) it is the scattering distribution which has an assumed Gaussian form (characterized by the distribution's standard deviation, σ).

This theory assumes that the air filling the interstitial space between the layer particles is transparent to the photons. Some of the photons entering the layer eventually, through scattering, are reemitted from the surface. Both the reemitted and reflected photons are measured in this project.

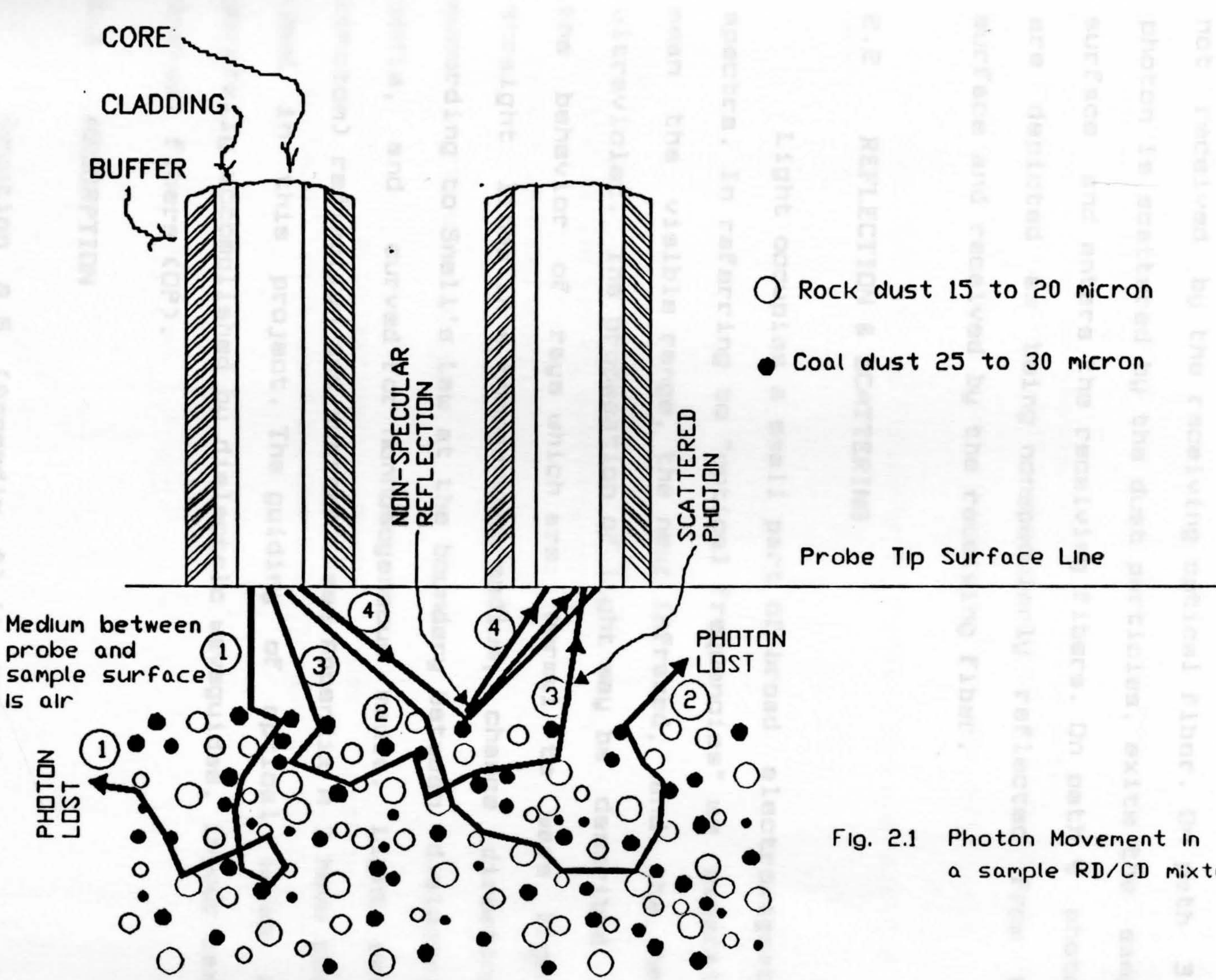

Fig. 2.1 Photon Movement in a sample RD/CD mixture.

The figure 2.1 depicts the motion of photons in a dust sample. Photons following trajectories 1 & 2 are scattered by the dust particles and are lost, i.e., they are not received by the receiving optical fiber. On path 3 a photon is scattered by the dust particles, exits the sample surface and enters the receiving fibers. On path 4 photons are depicted as being nonspecularly reflected from the surface and received by the receiving fiber.

2.2 REFLECTION & SCATTERING

Light occupies a small part of broad electromagnetic spectra. In referring to "optical frequencies" we generally mean the visible range, the near infrared, and the near ultraviolet. The propagation of light may be described by the behavior of rays which are: normal to wave front, straight lines in a homogeneous medium, change directions according to Snell's Law at the boundary between dielectric media, and curved for nonhomogeneous media. Light wave (photon) reflection and scatter (see Appendix A) have been used in this project. The guiding of optical waves is generally accomplished by dielectric waveguides, in our case optical fibers (OP).

2.3 ABSORPTION

Equation A.6 (Appendix A) is reproduced here as equation 2.1:

$$F = F_o e^{-\alpha_t d} \tag{2.1}$$

where,

$e = 2.718$

F_o is number of photons striking the surface, per unit time, per unit area.

F is the number of photons that survive after reflection/scatter and travel through a distance d.

α_t is the total absorption coefficient of the material.

Introducing coefficients of reflection and scatter we have,

$$\alpha_t = \alpha_r + \alpha_s \tag{2.2}$$

where,

α_r is the reflectivity coefficient

α_s is the scatter coefficient

2.4 MATHEMATICAL MODEL

The mathematical model, for photon flux backscattered, developed by the U.S. Bureau of Mines is[2]

$$F_w = X \cdot \left[\frac{\left(1 - \frac{\alpha_{rc}}{\alpha_{rr}}\right)}{(X + k(1-X))} \right] + \frac{\alpha_{rc}}{\alpha_{rr}} \tag{2.3}$$

where,

α_{rc} = coal dust particle reflectivity

α_{rr} = rock dust particle reflectivity

X = mass fraction of the rock dust

ρ_r & ρ_c are the particle densities of RD and CD, respectively

N_r & N_c are the RD,CD particle number density, respectively

R_r, R_c are the RD,CD effective particle radius, respectively

and,

$$k = \frac{R_r \rho_r}{R_c \rho_c} \tag{2.4}$$

Expanding equation (2.3) and after some manipulations, we obtain the following equation (2.5),

$$F_w = g(X) = a + \frac{bx}{c + Xd} \tag{2.5}$$

where,

$a = \frac{\alpha_{rc}}{\alpha_{rr}}$

$b = \left(1 - \frac{\alpha_{rc}}{\alpha_{rr}} \right)$

$c = k$

$d = (1 - k)$

$a + b = 1$

$c + d = 1$

Developing equation (2.5) further, we obtain

$$F_w = g(X) = \frac{\tilde{K} + XL}{c + Xd} \tag{2.6}$$

where,

$\tilde{K} = ac$

$L = ad + b$

Equation (2.6) is an 'improper rational function', this leads to a **hyperbola** which has an asymptotic behavior. If only a part of this hyperbolic function is considered, than it can be approximated with an exponential function. It is this assumption which is adapted in developing the related equations in this project.

2.5 BASIC EQUATIONS

Light travels in small bundles called **photons**. Since the reflection and scatter of photons from a dust surface is nonspecular, photons will be randomly reflected and scattered. $P(\theta)$ represents the random travel of the photons:

$$P(\theta) = N\, e^{-\frac{1}{2}\left(\frac{\theta}{\sigma}\right)^2} \qquad (2.7)$$

Inserting this probability factor in equation 2.1 we obtain,

$$F = F_o\, P(\theta)\, e^{-\alpha_l d}\, \alpha_s\, \Delta \qquad (2.8)$$

where Δ is the vector displacement of photon.

This equation is used to evaluate the data collected.

2.6 MEASUREMENTS

The operation of the RD meter is based on the measurement of infrared light backscattered from a sample of a mixture of light RD and dark CD particles. The amount of light received increases with an increase of the concentration of RD in the sample.

2.7 EXPECTED RESULTS

The data collected should exhibit the exponential decay predicted by above basic equations. The curves will decrease monotonically characterized by an absorption coefficient that is a function of reflectivity (α_r) and scatter (α_s) coefficients for the mixture.

CHAPTER 3

APPARATUS AND PROCEDURES

3.1 INTRODUCTION

This chapter deals with the description of the apparatus and electronics used in the experimentation; the optical fiber, the optical fiber probe, and the light source employed are described. Figure 3.1 shows the schematic of the complete experimental setup.

3.2 OPTICAL FIBER PROBE

The Optical Fiber Probe (OFP) was fabricated at the U.S. Bureau of Mines, Pittsburgh, Pennsylvania. The OFP (shown in figure 3.2) consists of two plastic blocks approximately 0.25 inch (6.35 mm) thick, 2 inches (50.8 mm) long and 0.4 inch (10.16 mm) wide. A 50 μm (micron) deep and 2 mm long groove was machined on the inside surface of the probe block. Two parts of the probe block can be taken apart and reassembled using two machine screws.

3.3 OPTICAL FIBERS

Initially, silicon Optical Fibers (OF) were selected. These OF had a core diameter of 100 μm, cladding diameter of

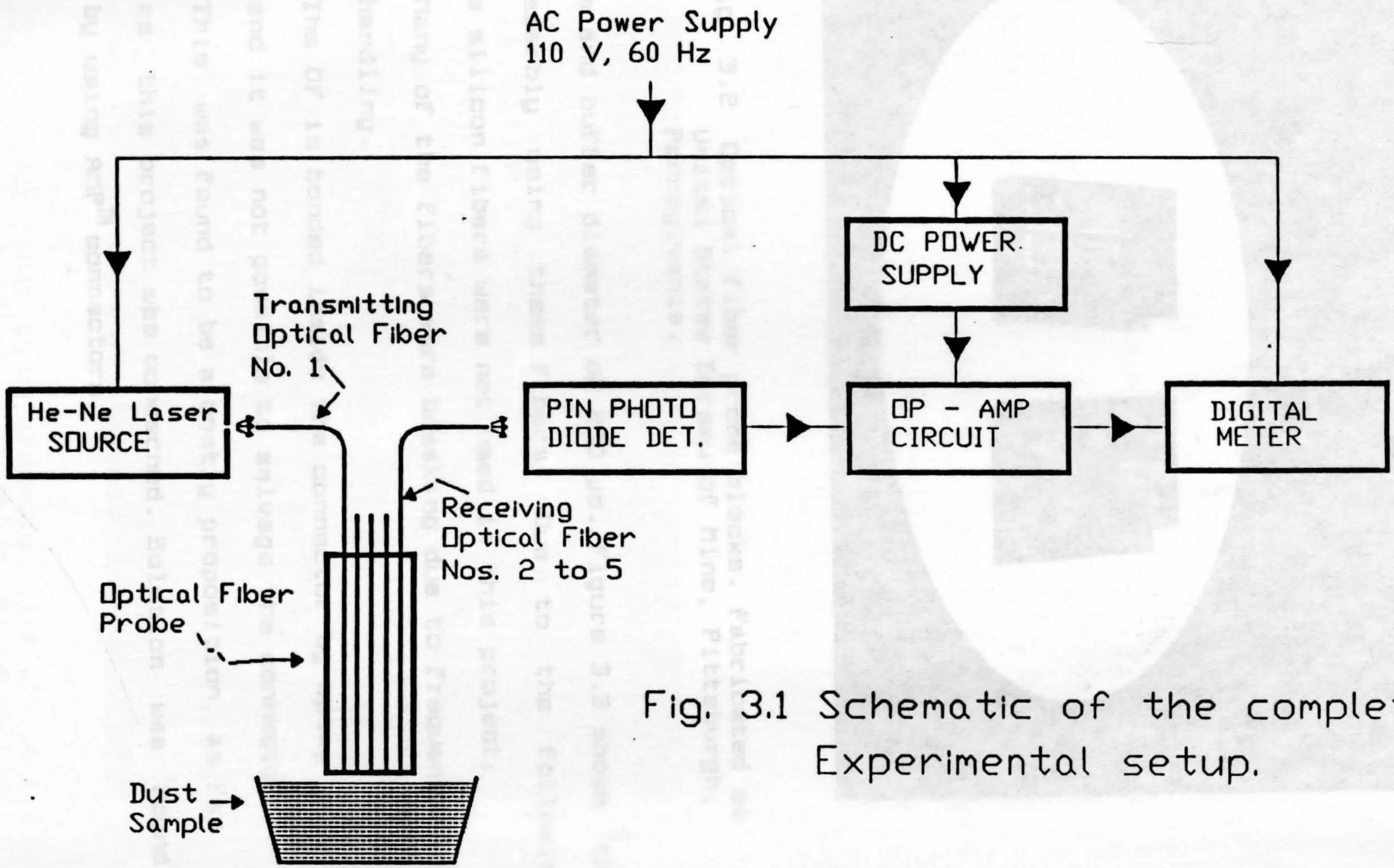

Fig. 3.1 Schematic of the complete Experimental setup.

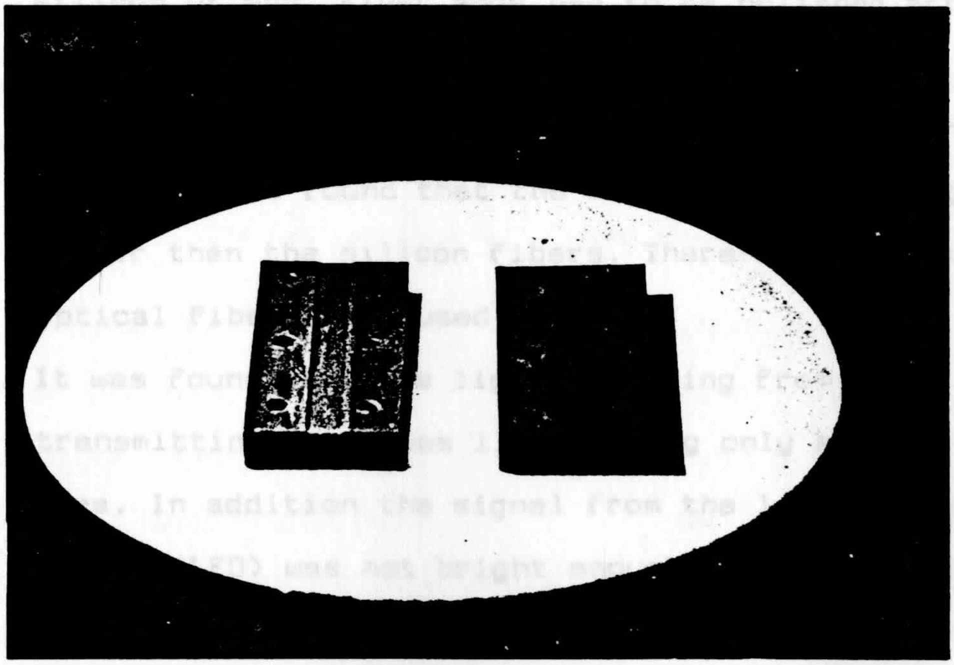

Fig. 3.2 Optical fiber probe blocks. Fabricated at United States Bureau of Mine, Pittsburgh, Pennsylvania.

140 µm and buffer diameter of 260 µm. Figure 3.3 shows the OFP assembly using these fibers. Due to the following reasons silicon fibers were not used in this project:

a. Many of the fibers were breaking due to frequent handling.

b. The OF is bonded inside the connector by epoxy and it was not possible to salvage the connector. This was found to be a costly proposition, as far as this project was concerned. Solution was found by using AMP™ connectors.

c. Another problem concerned the polishing of the silicon OF end. Fiber ends had to be polished after they were fitted between the OFP blocks. Silicon fibers are harder than the plastic material of the probe. It was found that the blocks were abrading faster than the silicon fibers. Therefore, plastic optical fibers were used.

d. It was found that the light emanating from the transmitting fiber was illuminating only a small area. In addition the signal from the light emitting diode (LED) was not bright enough for an equivalent output voltage to be measured.

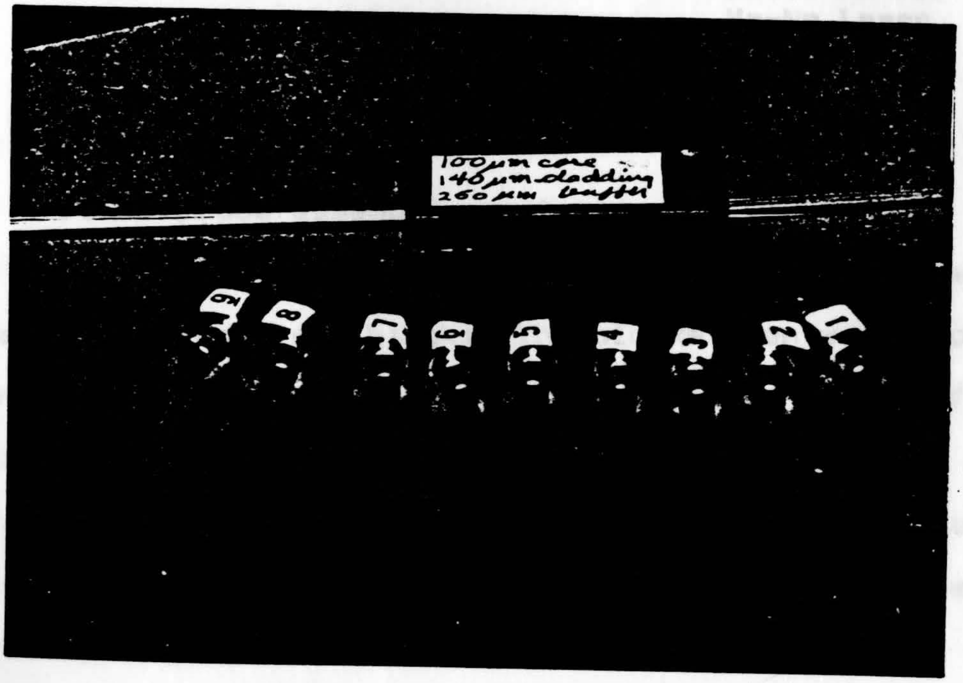

Fig. 3.3 Optical fiber probe assembly using 100 µm silicon optical fibers. This assembly was redesigned using five 1000 µm plastic fibers.

In view of the above points, selected ESKA™ plastic optical single fiber type EH 4001 (sample courtesy of Dr. Dominic Messuri of Packard Electric Division, Warren, Ohio). These OF has a core diameter of 1000 μm.

Typical Characteristic of Fiber used are:

Core Diameter	1000 μm
Outer Diameter	2200 ± 70 μm
Numerical Aperture (N.A)	0.47 ± 0.03
Critical Half-Angle θ_c	28°
Light Ray Acceptance Cone Angle	56°
Core Refractive Index	1.492 (n_1)
Sheath Refractive Index	1.417 (n_2)
Attenuation (dB/km) approx.	450 dB/km at 630 nm* * 632.8 nm for He-Ne Laser

3.4 PROBE ASSEMBLY

Final probe assembly consisted of five ESKA™ EH 4001 OFs. The fibers were laid side-by-side and sandwiched between the two probe blocks. The blocks then were screwed together (see figure 3.4), with the probe end of the fibers flush with the block end. Fibers were then polished using different grades of abrading paper. With the free end of the fibers illuminated the probes were checked under a microscope (courtesy of the department of Biology, KSU, Trumbull Campus). A circular light pattern seen under the microscope was a sufficient measure of good polished OF end.

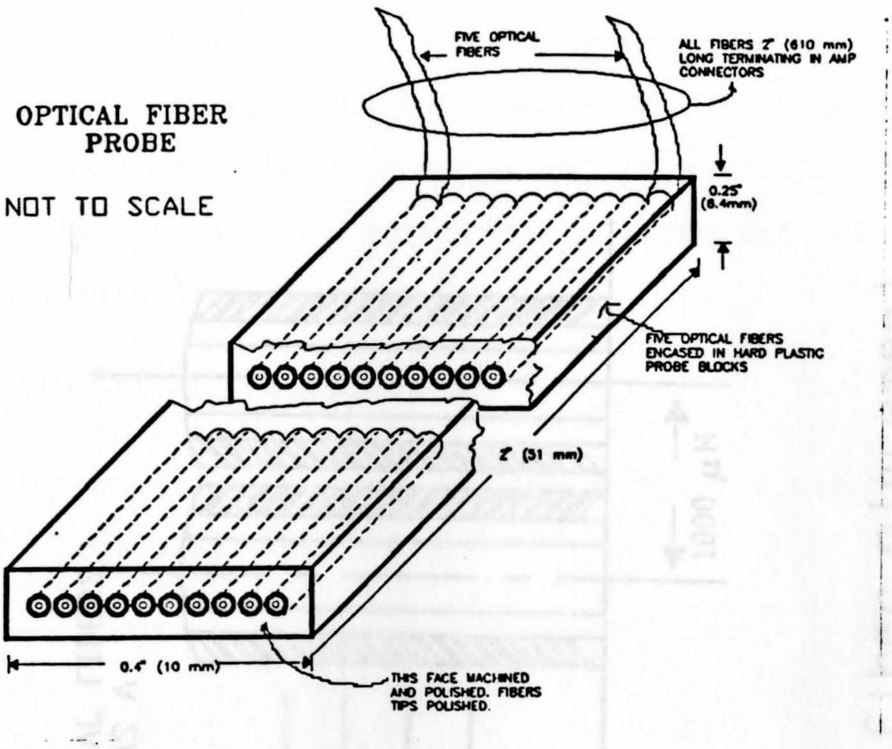

Fig. 3.4 Optical fiber probe assembly.

At the free end of the fibers AMP™ connectors were attached. One good thing about these connector was that no epoxy was required to fix the fibers, and they were reusable. Compared to other connectors these were much cheaper. The polishing procedure was also repeated at the connector. An enlarged view of the placement of fibers inside the probe is shown in figure 3.5.

3.5 THE ELECTRONICS

3.5.1 PHOTO DIODE

Photodiodes can be operated in two different modes to measure the light intensity, i.e., the reverse-biased mode and the short circuit mode[12].

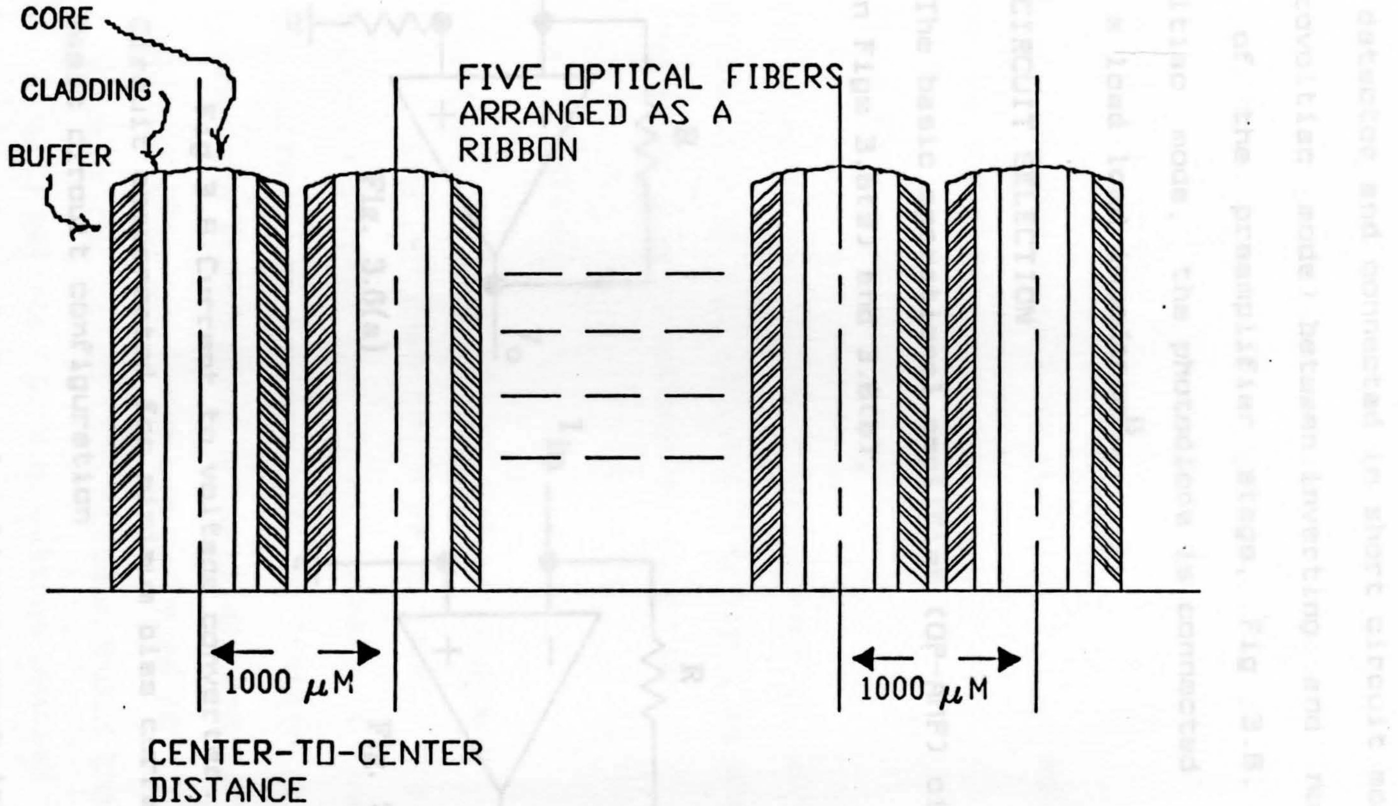

Fig. 3.5 Optical fiber placement inside the probe.

A Honeywell P-I-N photodiode HFD-3843-002 is used as a light detector and connected in short circuit mode (i.e., in photovoltiac mode) between inverting and noninverting inputs of the preamplifier stage, Fig 3.8. In the photovoltiac mode, the photodiode is connected without a bias to a load load impedance[13].

3.5.2 CIRCUIT SELECTION

The basic operational amplifier (OP-AMP) circuits are shown in Figs 3.6(a) and 3.6(b).

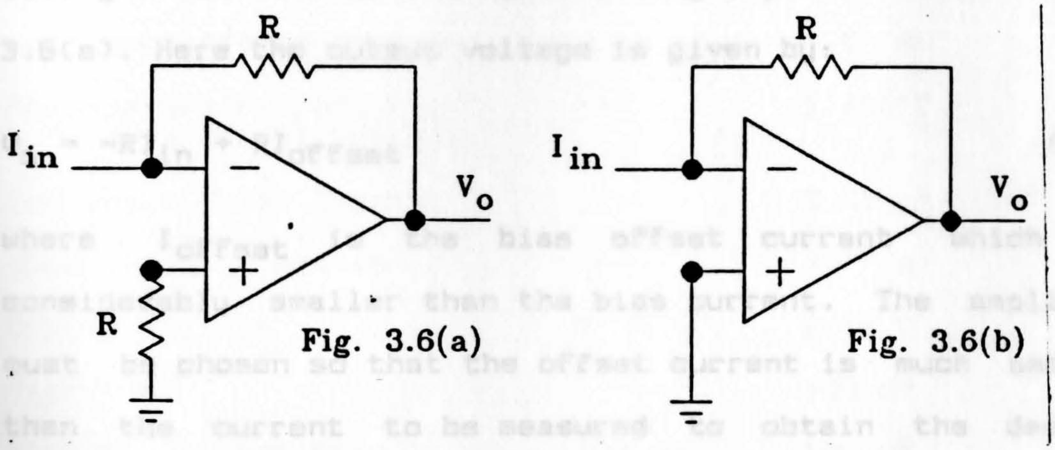

Fig 3.6 Current to voltage converter.

(a) Circuit compensated for minimum bias current error

(b) Basic circuit configuration

Under ideal conditions (no bias current infinite open loop gain and infinite impedance), the output voltage (V_o), is given by :

$$V_o = - RI_{in} \qquad (3.1)$$

and the output voltage is directly proportional to the current to be measured. The value of R is chosen so that the expected current produces the desired output. In our case a voltage of 200 mV is desired. For a current of 20 nA :

$$R = \frac{200 \times 10^{-3}}{20 \times 10^{-9}} = 10\ M\Omega$$

Since OP-AMPs draw bias current, I_{bias}, equation (3.1) must be modified:

$$V_o = -RI_{in} + RI_{bias} \qquad (3.2)$$

The error introduced by the bias current is minimized by adding a resistor to the noninverting input as shown in Fig 3.6(a). Here the output voltage is given by:

$$V_o = -RI_{in} + RI_{offset} \qquad (3.3)$$

where I_{offset} is the bias offset current which is considerably smaller than the bias current. The amplifier must be chosen so that the offset current is much smaller than the current to be measured to obtain the desired accuracy. For the measurement of nanoamps and picoamps it is usually necessary to use an OP-AMP with an FET input stage. Table 3.1 shows the comparison between Radio Shack's LM324 and Motorola's LF356 ICs. Offset voltage was set to obtain a zero output voltage, of the first stage, by adjusting the potentiometer R6 & R1 (see figure 3.8).

If the sensor is to be used over a wide range of temperatures, the leakage current can introduce considerable error. This problem is alleviated if the photodiode is used in the short circuit mode. With zero voltage across the diode there is no leakage current and the short circuit current is equal to the photodiode current I_{ph}. The circuit is as shown in Fig 3.7.

Table 3.1

Comparison of LM324 and LF356 OP-AMP ICs

	LM324	LF356
Type	-----	JFET
Low Input Bias Current	45 nA	30 pA
Low Input Offset Current	5 nA	3.0 pA
Low Input Offset Voltage	2 mV	1.0 mV
Temperature Compensation of Input Offset Voltage	-----	3 μV/°C
Low Input Noise Current	-----	0.01 pA/(Hz)$^{1/2}$
High Input Impedance	-----	10^{12} Ω
Supply Voltage	± 16 V	± 16 V
High CMRR	----	100 dB
High DC Voltage Gain	100 dB	106 dB

Source: Radio Shack & Motorola specification data sheets

In reality the amplifier offset voltage appears across the diode plus R_s. Since this voltage is very small, the leakage current is at least two orders of magnitude smaller than in the reverse bias mode. Neglecting the offset voltage, the output voltage of the amplifier is given by

$V_o = 2RI_{ph}$ (3.4)

Since resistor R is 10 MΩ the circuit's transconductance gain is 20 V/μA.

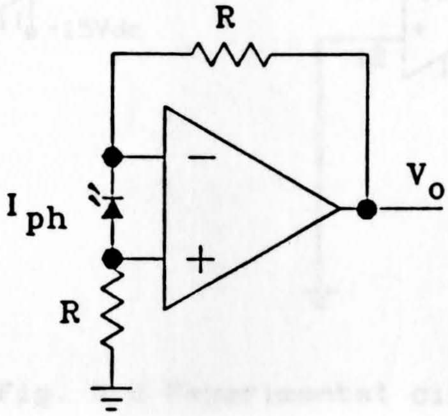

Fig. 3.7 Photodiode sensor amplifier for operation in the short circuit mode.

3.5.3 EXPERIMENTAL CIRCUIT

The experimental circuit is shown in Fig. 3.8. A Radio Shack IC QUAD OP-AMP LM324 was used for this feasibility study . All resistances used were ±1% metal film resistors to minimize temperature effects.

Since the equipment will be used both inside and outside of the mine, the circuit will be subjected to wide temperature variations. For this reason, the photodiode was used in short circuit mode. The IC LM324 has four OP-AMPs on the chip, but only two stages were used. This avoided unnecessary wiring, thereby reducing the noise picked up by long wires.

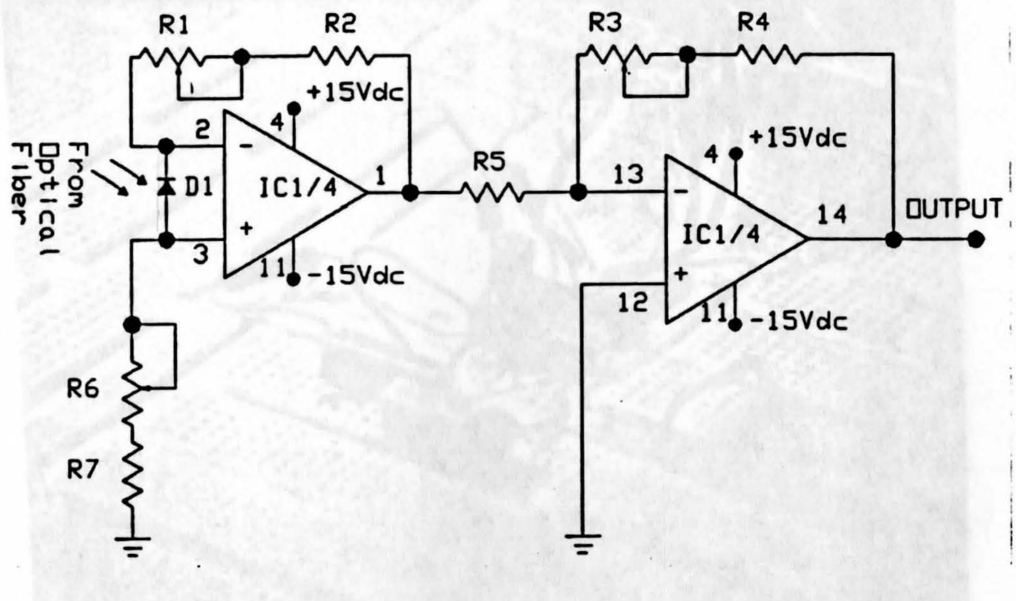

Fig. 3.8 Experimental circuit.

Component List:

D1	Photodiode, Honeywell HFD-3843-002
IC1	Quad OP AMP, Radio Shack LM324
R1,R6	1 MΩ, Variable Potentiometer
R3	150 KΩ, Variable Potentiometer
R2,R7	10 MΩ, ±1% Metal Film Resistor
R4	100 KΩ, ±1% Metal Film Resistor
R5	20 KΩ, ±1% Metal Film Resistor

A photograph of the circuit is shown in Fig. 3.9. Figure 3.11 shows the complete experimental set-up.

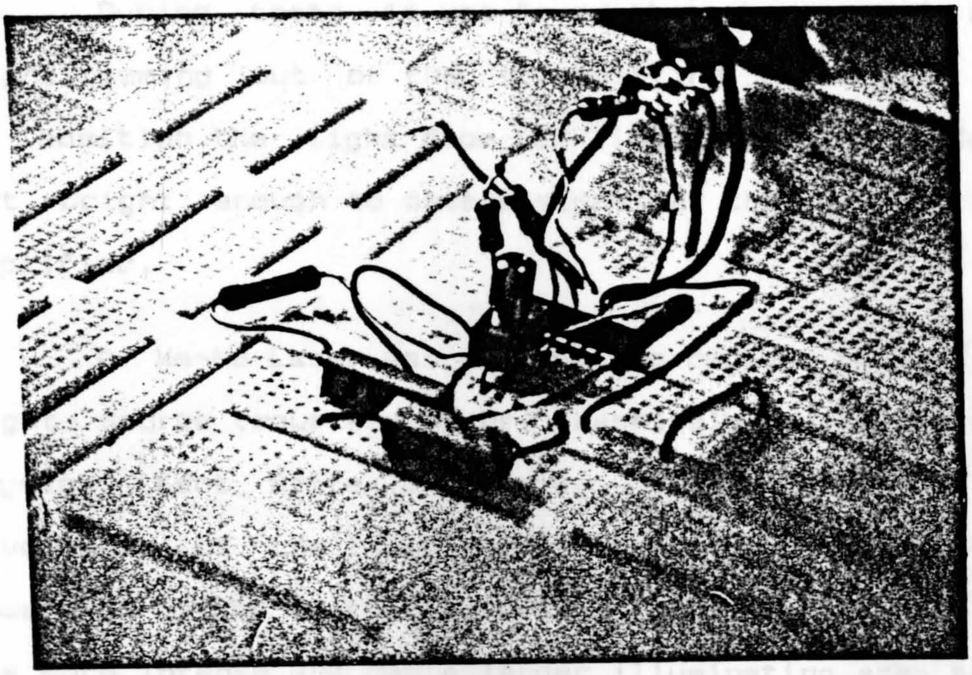

Fig. 3.9 Pictorial of actual circuit

3.6 NOISE

By connecting an oscilloscope at the output of the amplifier 1 MHz noise signal was observed. The source of this noise was not determined. The post-thesis plan includes determining and reducing this noise level.

Other sources of noise were due to the improper grounding of the breadboard and long device leads. Device leads could be trimmed, once the circuit is finalized and a proper printed circuit board is designed. The entire circuit could then be properly shielded.

3.7 LIGHT SOURCE

During tests it was found that the spread of the light coming out of the transmitting fiber was small. In addition the light from LED (light emitting diode) was not bright enough to obtain signal at the output of the amplifier.

A He-Ne Laser was obtained to replace the LED as a light source (courtesy of Dr. Shashikala Das, Professor of Physics, Kent State University, Trumbull Campus). The wavelength of the Laser was 632.8 nm (or 6328 Å). The power of light source was 0.95 mW (Fig. 3.10). The light was more intense and had a larger illuminating area than the LED. For the purposes of this preliminary investigation it was sufficient.

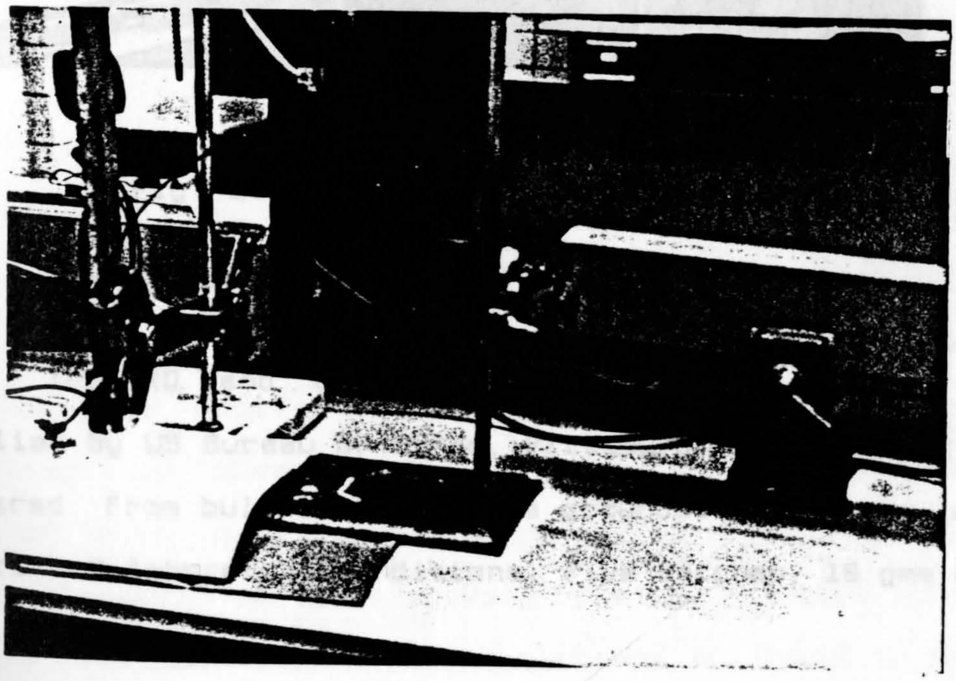

Fig. 3.10 He-Ne laser light source assembly.

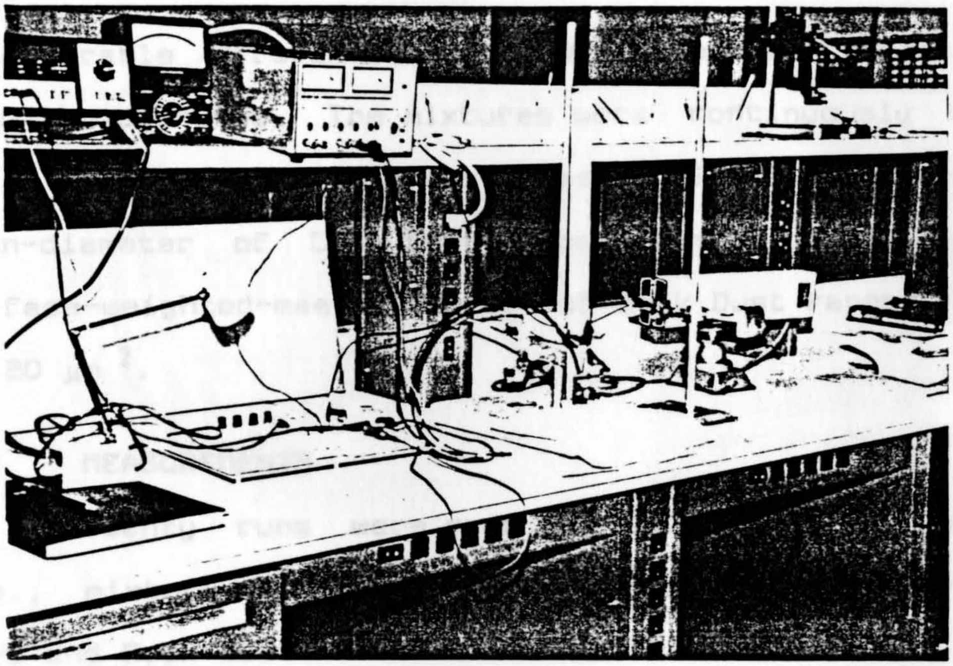

Fig. 3.11 General experimental setup.

3.8 SAMPLE MATERIAL

The RD and CD samples used in this project were supplied by US Bureau of Mines, Pittsburgh . Coal Dust was prepared from bulk coal that was grounded and sieved under controlled laboratory conditions. Five batches, 16 gms each of RD and CD mixtures were made:

100 %	Coal Dust
75% + 25%	Coal Dust (12 gms) + Rock Dust (4gms)
50% + 50%	Coal Dust (8 gms) + Rock Dust (8 gms)
25% + 75%	Coal Dust (4 gms) + Rock Dust (12 gms)
100%	Rock Dust

Considerable effort was made to ensure that the mixtures were homogeneous. The mixtures were continuously stirred until a uniform grayness was observed. The surface-weighted-mean-diameter of Coal Dust ranged from 25 to 30 μm. The surface-weighted-mean-diameter of Rock Dust ranged from 15 to 20 μm [2].

3.9 MEASUREMENTS

Twenty runs were made for each batch of samples, i.e., mixture of Coal Dust & Rock Dust and with pure Coal Dust and Rock Dust.

The light from the transmitting Fiber# 1 was irradiated on the surface of the sample. It was found during the experiment that immersing the probe into the mixture blocked the light and there was no measurable light coming out of the receiving fibers numbered 2 - 5. Due to electrostatic charge sample particles were clinging at the tip of both transmitting and receiving fibers; to avoid this, the probe was kept at some critical distance above the sample surface. This critical distance was found to be 3/8 inches (9.525 mm). This distance was found to give maximum possible voltage reading for corresponding light signal received in the respective receiving optical fibers. Figs. 3.12 and 3.13 show the reflected light picked up by the receiving optical fiber. Also, after every reading the probe surface was completely cleaned to remove any clinging dust particles.

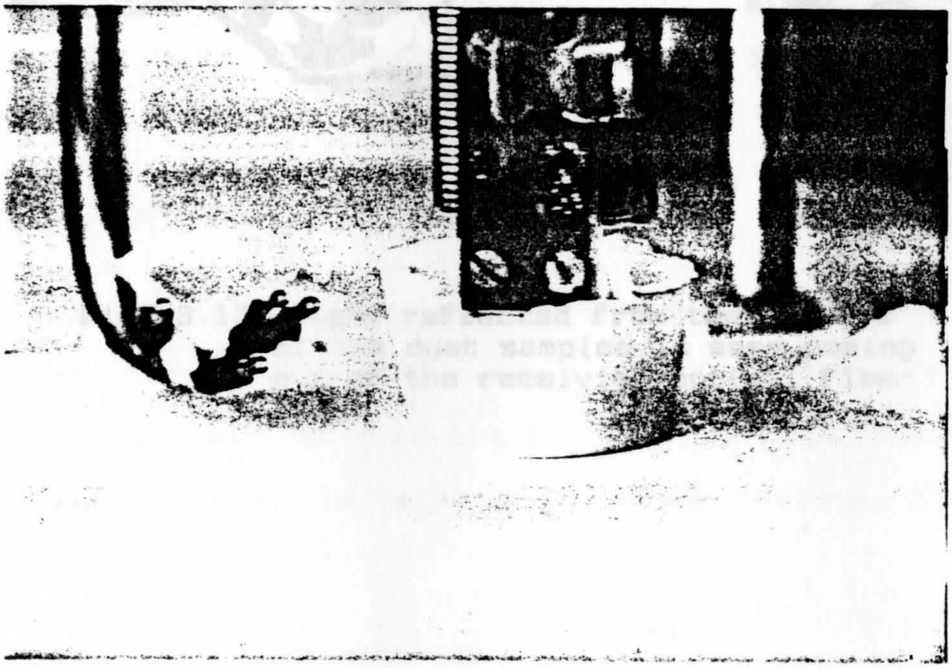

Fig. 3.12 Transmitting optical fiber illuminating the dust mixture.

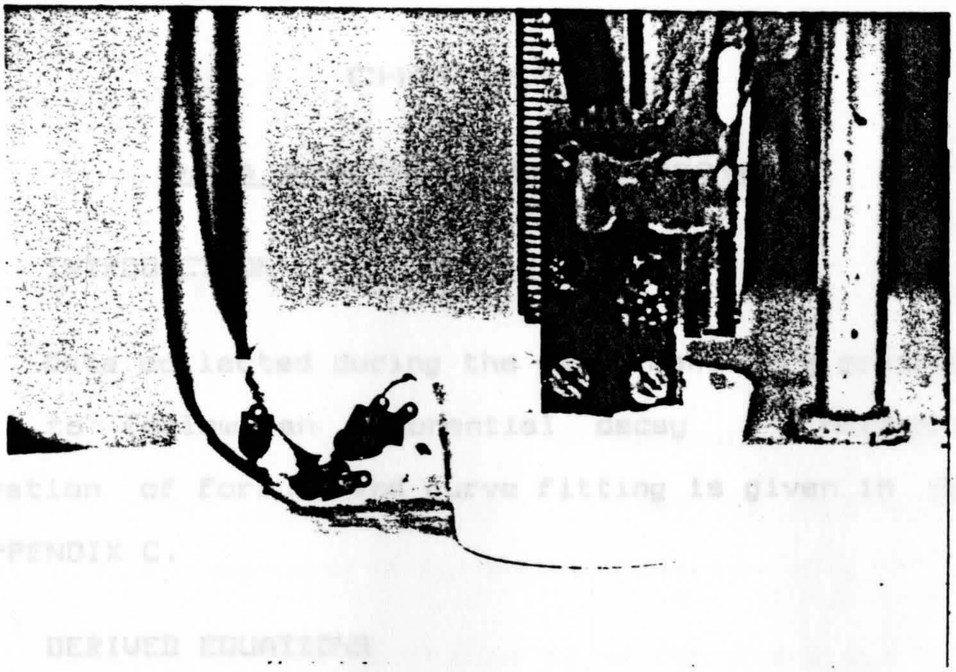

Fig. 3.13 Light reflected from the surface of the dust samples is seen coming out of the receiving optical fiber ends.

CHAPTER 4

DATA ANALYSIS AND DISCUSSIONS

4.1 INTRODUCTION

Data collected during the experiment were graphed and seem to follow an exponential decay . Mathematical derivation of formula and curve fitting is given in detail in APPENDIX C.

4.2 DERIVED EQUATIONS

Tables D.1 to D.5 (Appendix D) contains various data collected for different mixtures of the samples. Equations 4.1 to 4.5 are derived from the plots of the data (Appendix D) collected and the mathematical computations done in Appendix C.

For 100% Coal Dust + 0% Rock Dust

$$y = 8600\ e^{-4.2\cdot 10^{-3}x} \tag{4.1}$$

For 75% Coal Dust + 25% Rock Dust

$$y = 5100\ e^{-1.29\cdot 10^{-3}x} \tag{4.2}$$

For 50% Coal Dust + 50% Rock Dust

$$y = 9200\ e^{-1.47\cdot 10^{-3}x} \tag{4.3}$$

For 25% Coal Dust + 75% Rock Dust

$$y = 16400\ e^{-1.17 \cdot 10^{-3} x} \tag{4.4}$$

For 0% Coal Dust + 100% Rock Dust

$$y = 41900\ e^{-1.28 \cdot 10^{-3} x} \tag{4.5}$$

Setting $y = F$ and $x = d$, in equations 4.1 through 4.5, we express constant A as a function of parameters F_o, α_s and Δ; also, constant B is then a function of α_s.

Finally, actual constants to be found are α_t, α_s and α_r. These constants were not found and left out for future work, as this project was limited to the feasibility study for the development of a RD meter.

4.3 DATA ANALYSIS

Table 4.1 and figure 4.6 give the Output Voltage vs the RD percentages. The output voltage reading was from receiving fiber# 3. Measurements from other receiving fibers were discarded, because the output voltage was either saturated or near zero. This plot (figure 4.6) then could be used to determine the RD percentage corresponding to voltage measured at the output stage of the amplifier. The data indicates that grayness varies with RD percentage, i.e., the output of the amplifier varies with the percentage change in Rock Dust in a sample dust.

TABLE 4.1

Light Signal in Volts vs Rock Dust (in percent wt. pct).

	0%	25%	50%	75%	100%
01	0.0	0.395	0.568	2.100	2.600
02	0.0	0.260	0.445	1.860	3.300
03	0.0	0.312	0.543	1.780	2.300
04	0.0	0.555	0.605	2.020	1.760
05	0.0	0.585	0.641	1.910	1.580
06	0.0	0.264	0.568	1.790	1.600
07	0.0	0.455	0.615	1.830	1.670
08	0.0	0.122	0.511	1.930	2.500
09	0.0	0.482	0.452	1.720	2.040
10	0.0	0.469	0.790	1.630	2.090
11	0.0	0.366	0.678	1.730	1.320
12	0.0	0.465	0.535	1.810	2.480
13	0.0	0.402	0.533	1.830	2.300
14	0.0	0.273	0.535	1.820	1.670
15	0.0	0.344	0.770	1.690	2.720
16	0.0	0.321	0.740	1.780	2.180
17	0.0	0.378	1.035	1.810	2.220
18	0.0	0.365	0.458	1.740	2.460
19	0.0	0.199	1.090	1.690	3.280
20	0.0	0.554	0.650	1.650	2.060

Output taken off the number 3 receiving optical fiber

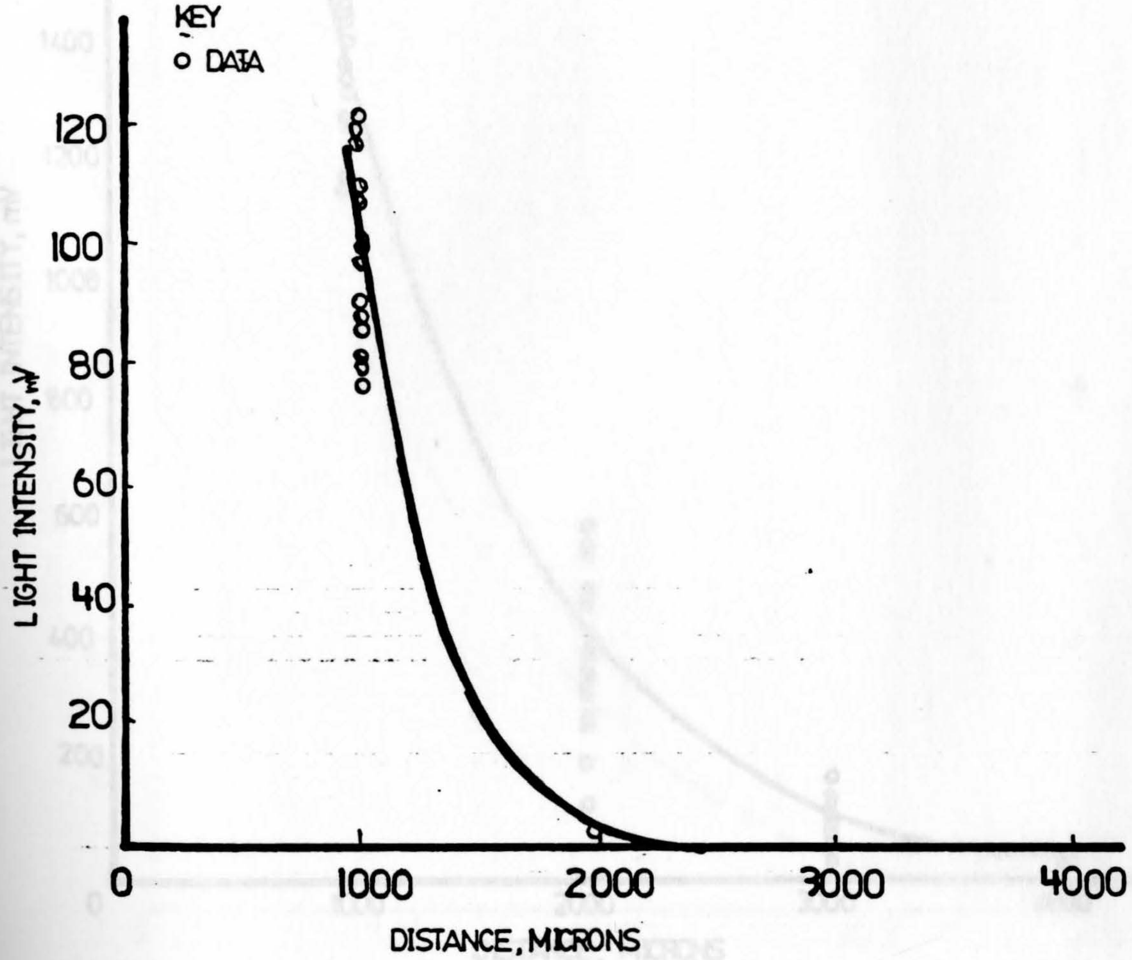

Fig. 4.1 Plot of Distance (μm) vs Output Voltage (mV) for 0% Rock Dust + 100% Coal Dust sample.

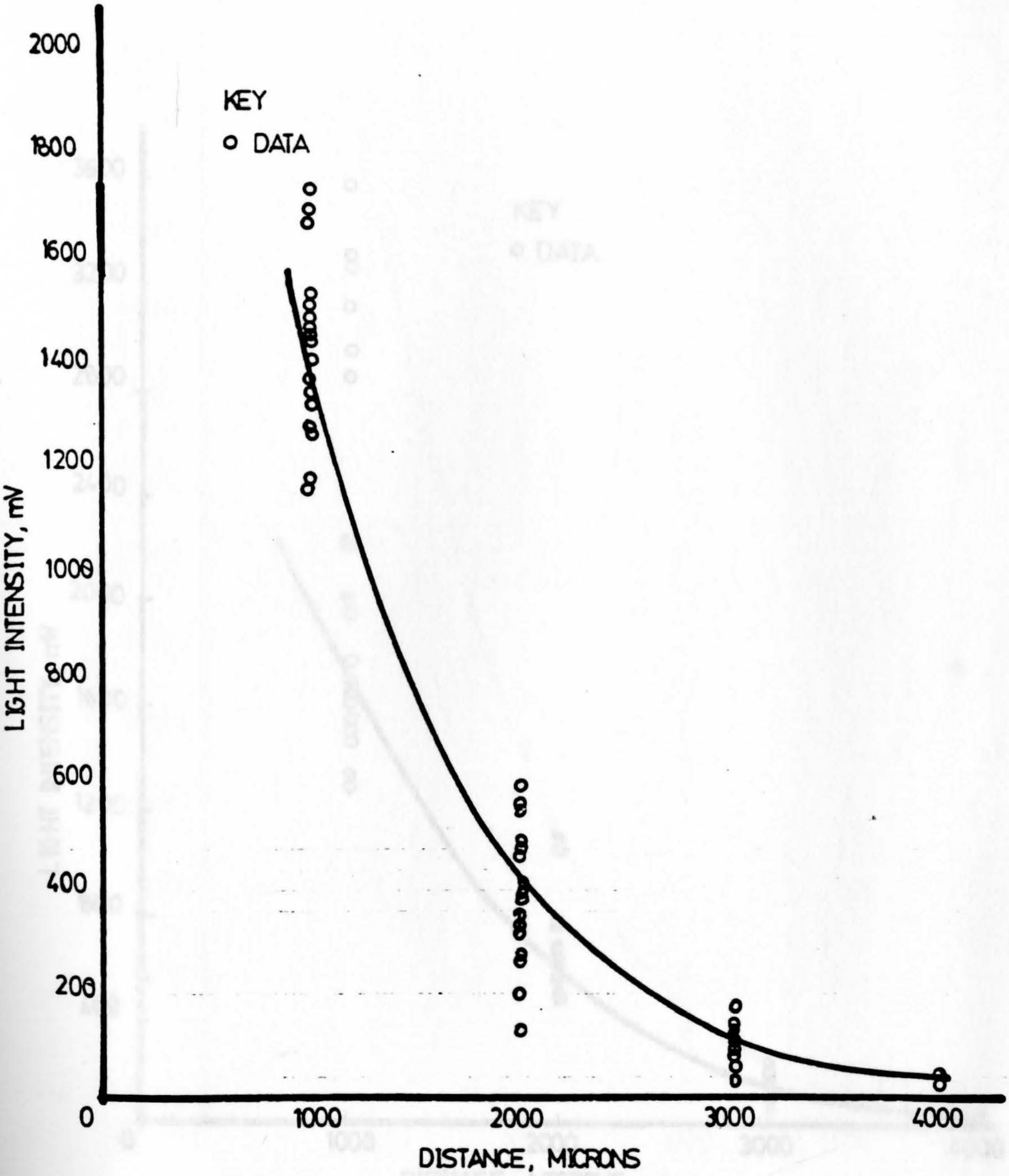

Fig. 4.2 Plot of Distance (μm) vs Output Voltage (mV) for 25% Rock Dust + 75% Coal Dust sample.

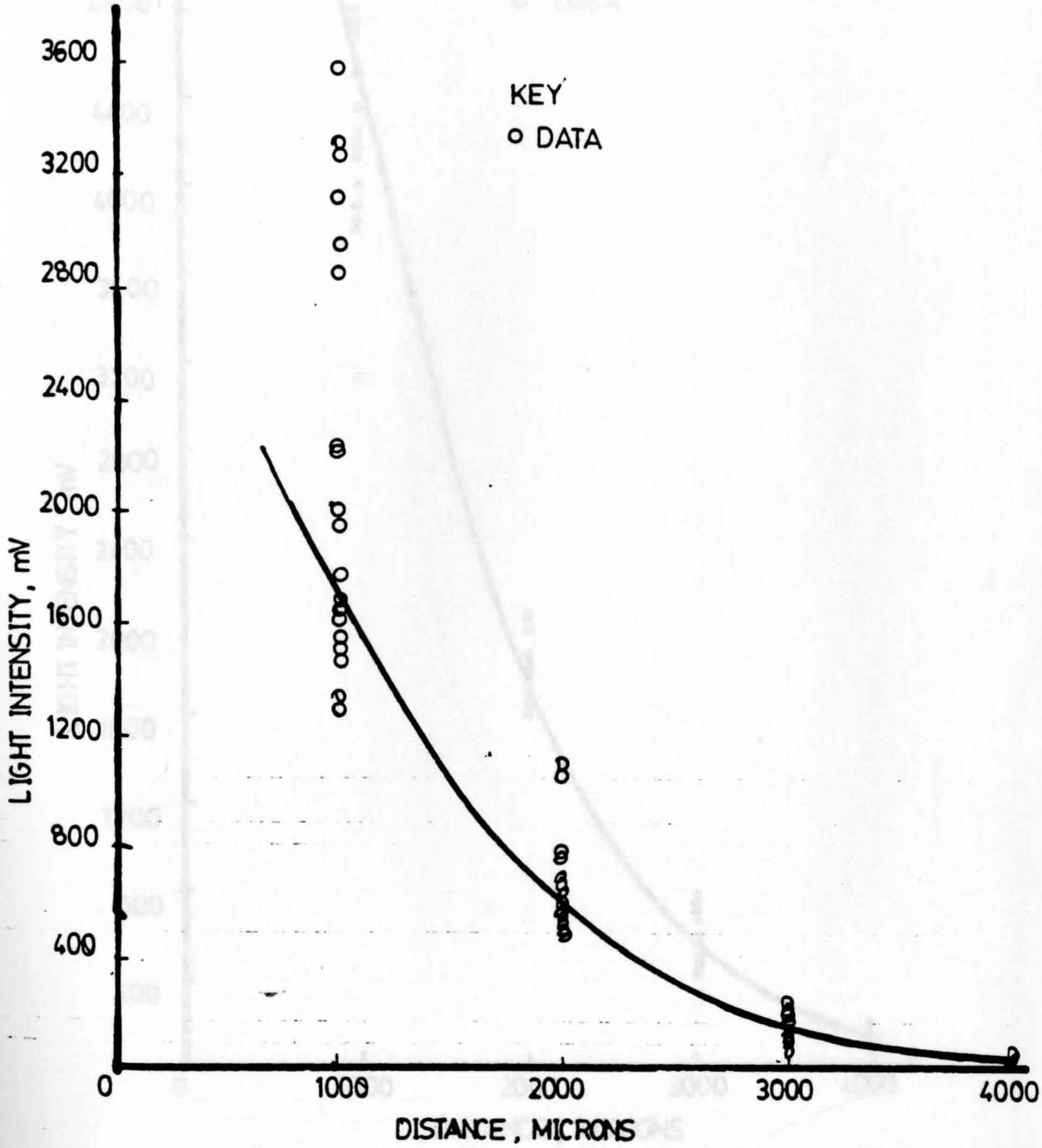

Fig. 4.3 Plot of Distance (μm) vs Output Voltage (mV) for 50% Rock Dust + 50% Coal Dust sample.

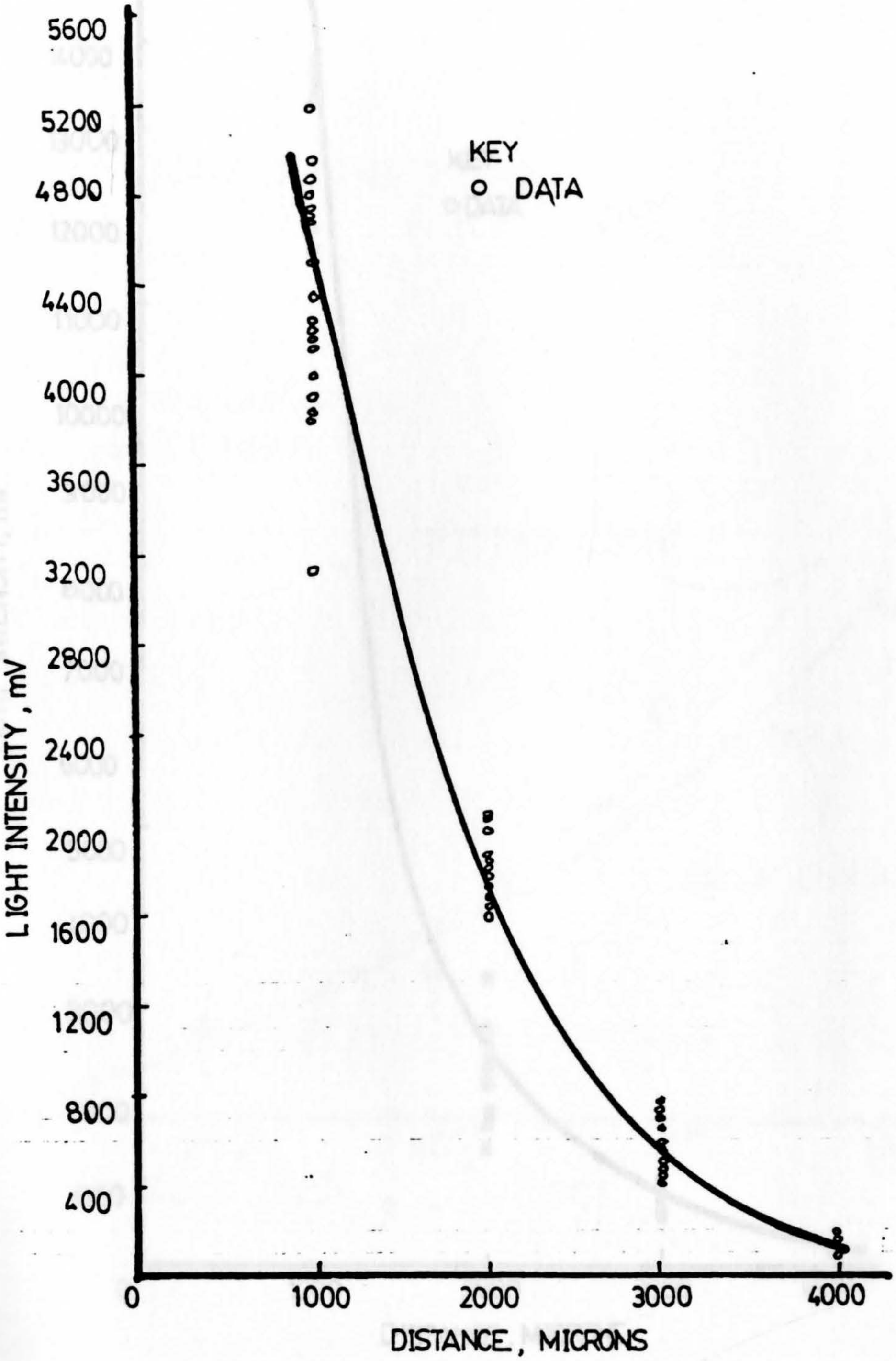

Fig. 4.4 Plot of Distance (μm) vs Output Voltage (mV) for 75% Rock Dust + 25% Coal Dust sample.

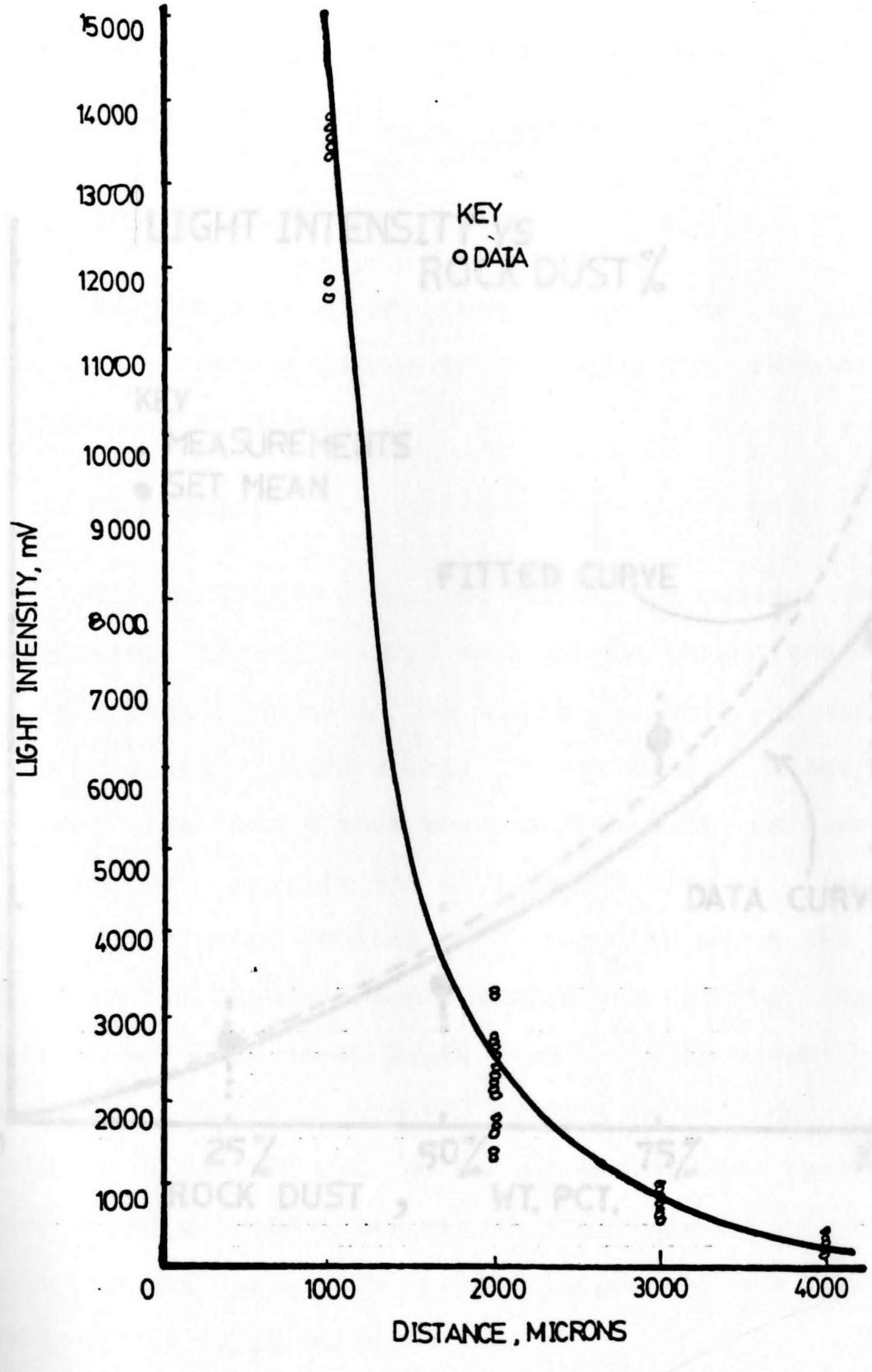

Fig. 4.5 Plot of Distance (µm) vs Output Voltage (mV) for 100% Rock Dust + 0% Coal Dust sample.

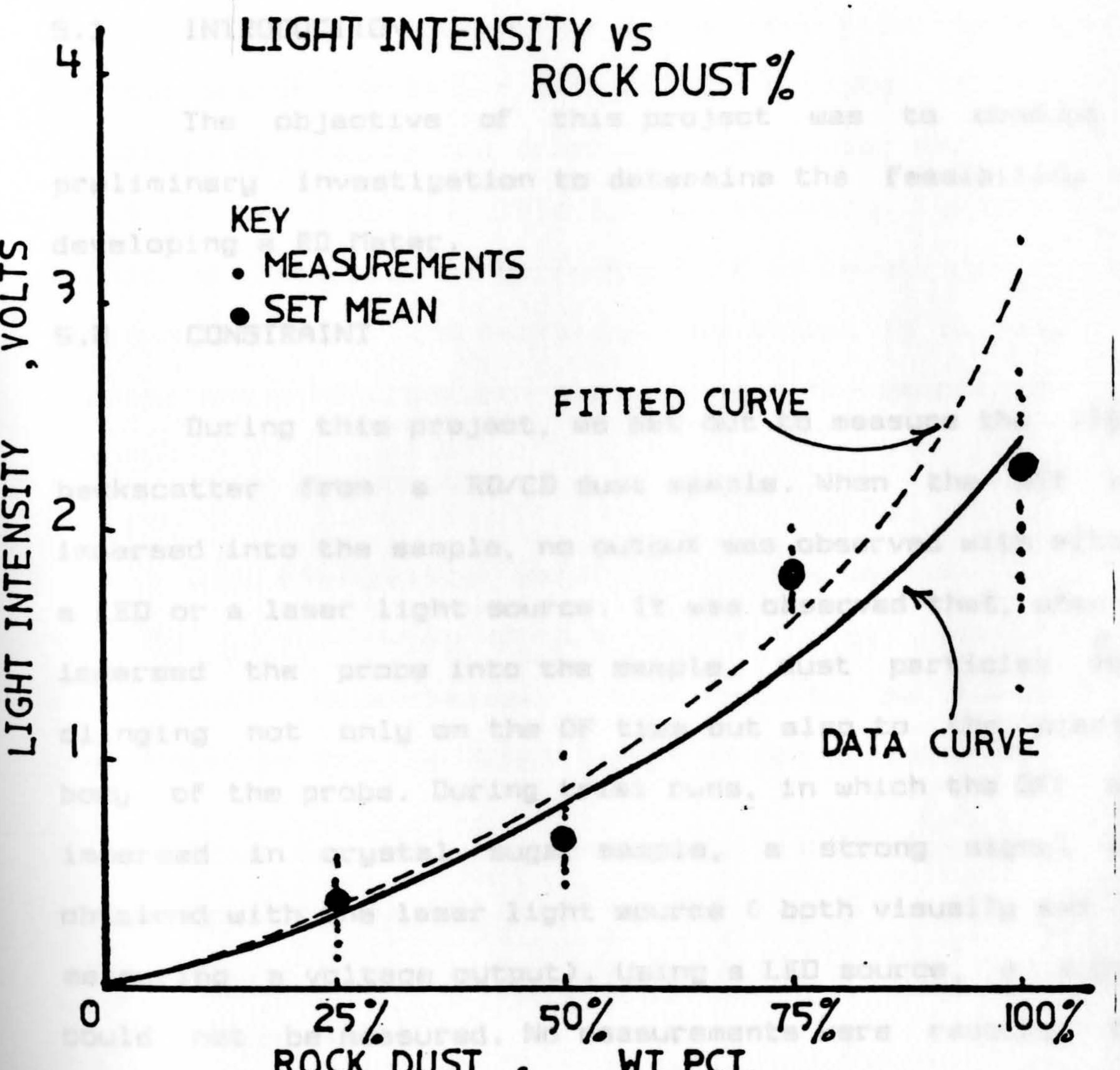

Fig. 4.6 Plot of RD percentage vs Output Voltage (Volts).

CHAPTER 5

CONCLUSIONS

5.1 INTRODUCTION

The objective of this project was to conduct a preliminary investigation to determine the feasibility of developing a RD Meter.

5.2 CONSTRAINT

During this project, we set out to measure the light backscatter from a RD/CD dust sample. When the OFP was immersed into the sample, no output was observed with either a LED or a laser light source. It was observed that, when we immersed the probe into the sample, dust particles were clinging not only on the OF tips but also to the plastic body of the probe. During trial runs, in which the OFP was immersed in crystal sugar sample, a strong signal was obtained with the laser light source (both visually and by measuring a voltage output). Using a LED source, a signal could not be measured. No measurements were recorded for this trial run. Does scatter in a particular medium depend on its crystal structure, material type and its reaction to the incident light (photon) ?

In view of the above observations, the strategy was changed during the course of this project. It was then limited to measure the reflection from the surface of the sample. The transmitting/receiving fibers (that is the OFP) had to be kept at some distance (see Chapter 3) above the surface of the sample.

Setting the distance of the optical fiber probe above the surface of the sample was not very precise. It was done manually by keeping the probe at a particular mark on the scale attached to the probe fixture assembly. Further, the sample surface was not perfectly flat or level. One way of reducing the error and variation this causes is to insert a transparent window between the probe and the sample surface.

5.3 OTHER CONSTRAINTS

The constraints mentioned in this section have no bearing on the theory of this project (i.e., scatter and reflection). Nevertheless, these have to be taken into consideration for the final design of the RD meter.

Other specific requirements for the design of the RD meter are listed below:

a. These constraints dictate a low noise high gain amplifier.

b. Battery operation and portability precludes the use of laser light source, as this requires a high voltage power supply. High voltages should not be used, since they could spark a fire or explosion.

c. Since the portability of the instrument is desired, search for high intensity LED has to be made.

5.4 ELECTRONICS

Another factor to be considered is that in the preamplifier stage FET OP-AMP was not used. The OP-AMP used had a higher input bias current than FET OP-AMP. It was observed that workbench power points may not be properly grounded. This might have introduced some noise.

5.5 EVALUATION

An evaluation of the data collected indicates that it is feasible to design such a meter. It is dependent on better data collection technique and instrumentation. It was found that the variation in light signal is dependent on the concentration of RD in a RD/CD mixture. Similar results were reported by US Bureau of Mines[2].

5.6 RESULTS

It was observed that, with the different mixtures of Coal Dust with Rock Dust, grayness of the test samples changes. With pure Rock Dust (whitish gray) the signal was very high and it was very low (practically zero) for pure Coal Dust (jet black). It can be concluded that there may be a relationship between the grayness of the sample and the percentage of RD in a particular sample by measuring the output signal. The RD meter's scale (digital or analog) can be calibrated in terms of RD percentage. Table 5.1 (based on the fitted curves) compares the test data with the fitted data. The information in Table 5.1 is limited to the output from optical fiber# 3.

TABLE 5.1

Light Intensity vs % of Rock Dust
(measured from OF# 3).

RD %	TEST DATA y_i mV	EXPONENTIAL FIT $(y_F)_i$ mV
0	0	0
25	300	390
50	700	490
75	1400	1600
100	2400	3240

CHAPTER 6

FUTURE WORK

Based on this project and the study of Optical Fibers, future work on the following projects could be of interest,

1. Measurement of dust particle concentration in surrounding air using optical fibers. This will be of special interest to Hospitals and Clean Rooms. Principle to be used is light scatter from the dust particles.

2. When a material is subjected to an electric field, its refractive index changes. Since optical fibers are considered dielectric waveguides, we can expect a change in their refractive index. This change in refractive has direct relationship with the light wave transmission inside of the fiber. This effect could be utilized in designing a sensor to measure high currents inside the electric machines.

3. A change in diffraction and phase pattern is produced in an optical fiber, when subjected to sound (acoustic) waves, due to photoelasticity. This effect can be used to modulate a light beam in the optical fiber. Many properties, e.g., light conducting velocity, reflection and transmission coefficients

at interfaces, acceptance angles, and transmission modes are dependent upon the diffractive changes occurring in the optical fiber.

4. A simple optical fiber temperature sensor, which could be attached on the surface of the boiler or inside an electric generator. The temperature sensed could then be used as a control signal. There are various ways by which this could be achieved. When two fibers are coupled, there could be a mismatch between the fiber ends. This mismatch could result in the attenuation of the light signal. What is then needed is to artificially create this mismatch and relate this to variation in the temperature.

APPENDIX A

RAY AND WAVE OPTICS

A.1 REFLECTION

When light strikes an object the light is transmitted (refracted) through , absorbed by, or reflected from the object. Reflection can be said to be either SPECULAR or NONSPECULAR.

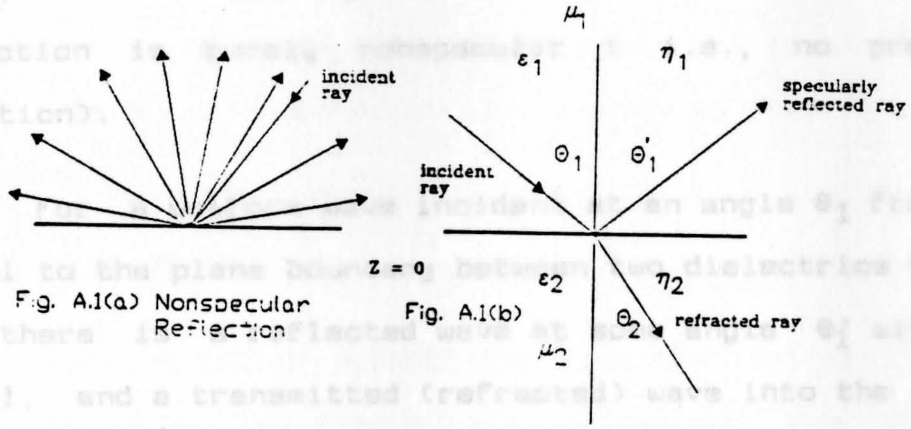

Fig. A.1 Specular, nonspecular reflection and refraction.

In fig. A.1a, an incident ray of light strikes a surface and is reflected nonspecularly. In a pure nonspecular reflection, the reflected rays go in all directions with equal intensities. Most of the light detected by our eyes has undergone a nonspecular reflection.

In fig. A.1b, an incident ray of light undergoes a specular reflection at a surface. In a pure specular reflections, all of the reflected light travels in one definite direction. The **angle of incidence** θ_1 (measured between the incident ray and the normal to the surface) equals the **angle of reflection** θ_1' (measured between the reflected ray and the normal to the surface). In specular reflection

$$\theta_1 = \theta_1' \qquad (A.1)$$

No reflection is exactly a specular reflection (i.e., 100% of the light in one direction), and also, no reflection is purely nonspecular (i.e., no preferred direction).

For a uniform wave incident at an angle θ_1 from the normal to the plane boundary between two dielectrics ϵ_1 and ϵ_2, there is a reflected wave at some angle θ_1' with the normal, and a transmitted (refracted) wave into the second medium which is drawn at some angle θ_2 with the normal. For either type of polarization, the continuity condition on tangential components of electric and magnetic fields at the boundary $z=0$ must be satisfied for all values of x. As in the case of reflection from the perfect conductor, this is possible for all values of x only if incident, reflected, and refracted waves all have the same phase factor with respect to the x direction.

Thus,

$$k_1 \sin\theta_1 = k_1 \sin\theta_1' = k_2 \sin\theta_2 \,; \tag{A.2}$$

for vacuum or air,

$$\epsilon_0 = 8.854 \times 10^{-12} \approx \frac{1}{36\pi} \cdot 10^{-9}\ \mathrm{F/m}\ ;\ \text{and} \tag{A.3}$$

for other materials,

$$\epsilon = \epsilon_r\, \epsilon_0 \tag{A.4}$$

The first pair in equation (A.2) gives the result $\theta_1 = \theta_1'$ (the angle of reflection is equal to the angle of incidence).

A.2 REFRACTION

SNELL'S LAW OF REFRACTION: From the last equality the equation (A.2), we find a relation between the angle of refraction θ_2 and the angle of incidence θ_1:

$$\frac{\sin\theta_2}{\sin\theta_1} = \frac{k_1}{k_2} = \frac{v_2}{v_1} = \frac{n_1}{n_2} \tag{A.5}$$

This relation is known as Snell's Law. The refractive index n is defined to be unity for free space. For most dielectrics, n_1/n_2 may be replaced by $(\epsilon_1/\epsilon_2)^{1/2}$ since $\mu_1 = \mu_2 = \mu_3$.

A.3 ABSORPTION

Whenever a beam of particles strikes a barrier, the particles interact with the atoms in the barrier material. The thicker the material, the more likely it is that an incident particle interacts with an atom. The actual type of interaction depends on the type and energy of the incident particle and the material the barrier is made of, but the net effect is that fewer and fewer of the original particle, continue through the material. The barrier device is often called an **ABSORBER**.

The number of incident particles striking a surface per unit time per unit area is F_o, and the number of these particles per unit time, per unit area, that survive after traveling through a thickness L of the absorber is denoted by F. The relationship between F_o, F and L is given by the equation:

$$F = F_o\, e^{-\alpha_t L} \qquad \text{(A.6)}$$

where e = 2.718 and α_t is the **ABSORPTION COEFFICIENT** of the material. The **ABSORPTION COEFFICIENT** depends on the type of incident particle, the energy of incident particle, and the material of which the barrier is made ; that is,

$$\alpha_t = \left(\frac{-1}{L}\right) \ln \left(\frac{F}{F_o}\right) \qquad \text{(A.7)}$$

The process whereby the intensity of a beam of

Electromagnetic radiation is attenuated in passing through a material medium by conversion of the energy of the radiation to an equivalent amount of energy which appears within the medium, the radiant energy is converted into heat or some other form of molecular energy.

A perfectly transparent medium permits the passage of a beam of radiation without any change in intensity other than that caused by the spread or convergence of the beam, and the total radiant energy emergent from such a medium equals that which entered it, whereas the emergent energy from an absorbing medium is less than that which enters, and in the case of highly opaque media, is reduced practically to zero.

No known medium is opaque to all wavelengths of the Electromagnetic spectrum, which extends from radio-waves, whose wavelengths are measured in kilometers, through the infrared, visible and ultraviolet spectral regions, to X rays, of wavelengths down to 10^{-11} cm. Similarly, no material medium is transparent to the whole electromagnetic spectrum. A medium which absorbs a relatively wide range of wavelengths is said to exhibit **general absorption**.

A.4 THE PHOTONS

Light travels in small bundles called **PHOTONS**. **PHOTON** is a portion of a wave that contains only a definite number of cycles (not infinitely long). Energy is transported by electromagnetic pulses. Each PHOTON has a definite amount of energy that is related to its frequency by the relationship :

$$E = hf \qquad (A.8)$$

where h is the Planck's constant ($= 6.626 \times 10^{-34}$ Joules.s or $= 4.141 \times 10^{-15}$ eV.s (1 eV $= 1.60 \times 10^{-19}$ Joules).

A.5 LIGHT WAVE PROPAGATION AND SCATTERING

Wave propagation and scattering has great significance in communication, remote-sensing and detection. Media may vary in time and space, thereby the amplitude and phase of light waves may also fluctuate randomly.

APPENDIX B

OPTICAL FIBERS

B.1 OPTICAL FIBERS - BASIC ADVANTAGES

Compared to other systems, optical fiber transmission systems have unique advantages, as listed below:

a. operate with less energy per message unit-mile,

b. lower signal attenuation per unit distance,

c. higher bandwidth,

d. lower electromagnetic interference,

e. lower cross-talk,

f. higher resistance to clandestine eavesdropping,

g. lower shock hazard,

h. smaller size,

i. less weight, and

j. reduced consumption of critical metals,

k. operable under hazardous conditions, like mines, and inflammable environment

The optical signal may be in analog or discrete form and the system may operate with or without optical-to-electrical or electrical-to-optical signal conversion.

B.2 DESIGN OBJECTIVES

Some of the design objectives considered in the development of a good optical fiber are illustrated in fig. B.1. The system consists of an optical source . The

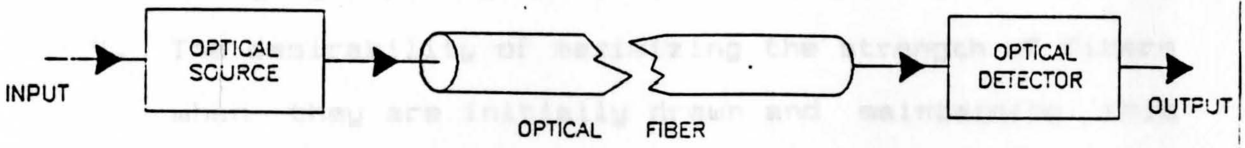

Fig. B.1

input signal at the left represents the information that is impressed on the light beam that, after emerging from the source, is focused into one end of an optical fiber. The light travels through the fiber and emerges from the opposite end, where it is directed into an optical detector.

Four major design objectives are:

1. The desirability of maximizing the amount of available light that is coupled/transferred into the core of the fiber. It is only the light in the core that is propagated along the length of the fiber with relatively low optical power loss. In order to maximize the amount of light transferred into the core, it is necessary to maximize the numerical aperture (N.A.) of the fiber.
2. The desirability of minimizing the light lost from a beam as it travels through the core from the input to the output end of the fiber. This light loss is

called the attenuation (power loss) rate, expressed usually in dB per kilometer of fiber.

3. The desirability of maximizing the information-carrying capacity of the fiber.
4. The desirability of maximizing the strength of fibers when they are initially drawn and maintaining this strength when the fibers are formed into cables or are used in sensors.

B.3 BASIC THEORY

According to the theory of light, a ray incident from below on the interface between two transparent media, at an angle θ_1 with the interface surface behaves as shown on fig. B.2 . When angle θ_1 is large, part of the incident beam is transmitted into the upper medium 2 and part is reflected back into medium 1. Their relative intensities depend upon the refractive indices of the two media.

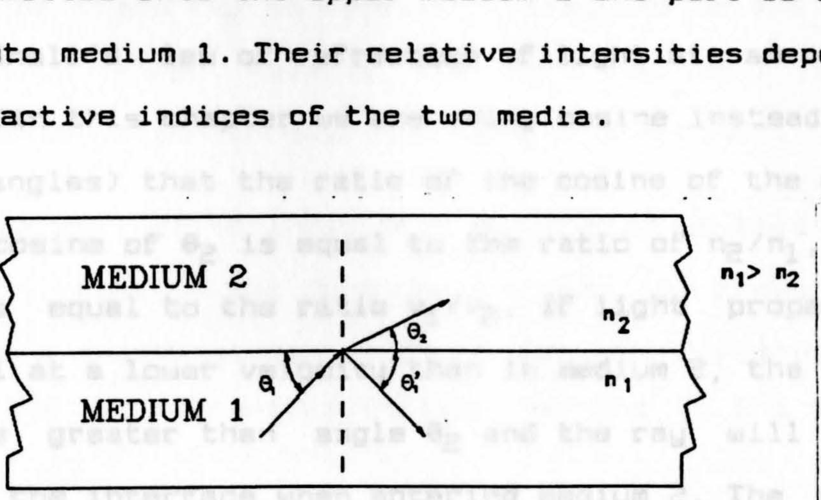

Fig. B.2 Reflection and refraction at the interface when a light wave travels from a higher to a lower refractive index medium.

The refractive index of a medium is defined as the ratio of the velocity of light in a vacuum to the velocity of light in the medium. The higher the refractive index of a medium, the slower light will travel in it. The refractive index of medium 1 is designated as n_1 and that for medium 2 as n_2, as shown in the figure B.3.

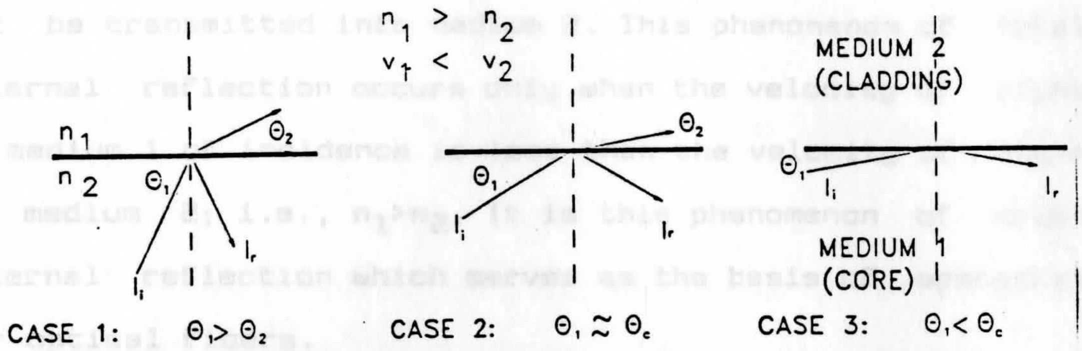

Fig. B.3 Internal reflection of light rays striking an interface surface at angles greater than, less than, and at, the critical angle.

Snell's law of refraction of light at an interface states (in this chapter we are using cosine instead of sines of the angles) that the ratio of the cosine of the angle θ_1 to the cosine of θ_2 is equal to the ratio of n_2/n_1, which in turn is equal to the ratio v_1/v_2. If light propagates in medium 1 at a lower velocity than in medium 2, the angle θ_1 will be greater than angle θ_2 and the ray will be bent toward the interface when entering medium 2. The angle of the reflected beam is equal to the angle of incidence. As the angle θ_1 is progressively decreased, a state will reach that beyond which the beam will be totally reflected back into the medium 1. This angle at which the total internal reflection occurs is called the critical angle. Let that angle be designated as θ_c, where θ_1 is equal to θ_c.

$$\theta_c = \cos^{-1}\left(\frac{n_2}{n_1}\right) \qquad \text{(B.1)}$$

For all values of θ_1 equal to or less than the critical θ_c, the incident ray will be totally reflected and energy will not be transmitted into medium 2. This phenomenon of total internal reflection occurs only when the velocity of light in medium 1 of incidence is less than the velocity of light in medium 2; i.e., $n_1 > n_2$. It is this phenomenon of total internal reflection which serves as the basis of operation for optical fibers.

The refractive index of the core material must be slightly higher than that of the cladding material. In this manner, the light ray is totally trapped inside the core of the optical fiber. Ideally, the light ray will propagate without attenuation through the core of the fiber.

The refractive index of the cladding is held slightly less than that of the core and thus it is convenient to introduce a quantity, say Δ, the fractional difference between the two refractive indices, defined by the equation:

$$\Delta = (n_1 - n_2)/n_1 \qquad \text{(B.2)}$$

From Equation (B.1) and (B.2), and for a ray that travels in a plane containing the central axis of the core (a meridional ray), the cosine of the critical angle is given by $\frac{n_2}{n_1}$; that is,

$$\cos\theta_c = \frac{n_2}{n_1} = 1 - \Delta \tag{B.3}$$

$$\cos^2\theta_c = 1 - 2\Delta + \Delta^2 \tag{B.4}$$

$$\sin^2\theta_c = 1 - \cos^2\theta_c = 2\Delta - \Delta^2 \tag{B.5}$$

$$\sin\theta_c = (2\Delta - \Delta^2)^{\frac{1}{2}} \tag{B.6}$$

when $\Delta << 2$, which is usually the case for optical fibers, then:

$$\sin\theta_c \cong \sqrt{(2\Delta)} \tag{B.7}$$

Critical angles, as θ_C, are usually only a few degrees in measure. Rays propagating inside the core at angles equal to or less than θ_C will be trapped inside the core, while rays that propagate at angles $\theta_1 > \theta_C$ will be partially transmitted into the cladding each time they encounter the core-cladding interface. These rays rapidly attenuate as they travel further into the core and thus do not contribute significantly to propagation over long distances.

B.4 NUMERICAL APERTURE (N.A.)

The numerical aperture (N.A.) of an optical fiber is defined as the sine of half angle of the cone of light that is incident from air on the input end of an optical fiber, such that all the rays having a direction that lies within such that all the rays having a direction that lies within the cone will be trapped within the core once they enter the fiber as shown in fig B.4.

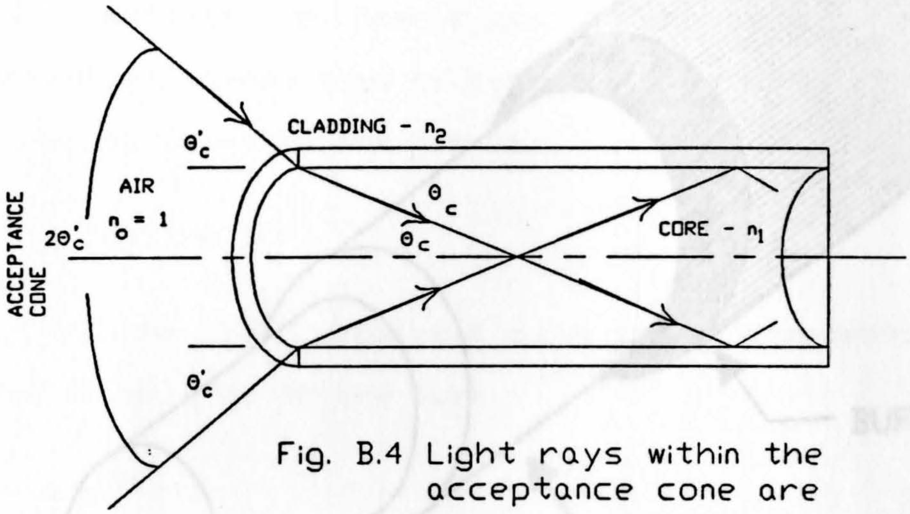

Fig. B.4 Light rays within the acceptance cone are trapped within the core.

From the definition, numerical aperture (N.A.) is equal to sin θ'_c:

$$N.A. = \sin\theta'_c = \sqrt{\left(n_2^2 - n_1^2\right)}, \text{ or} \tag{B.8}$$

$$N.A. \approx \sqrt{\left[2n_1(n_1 - n_2)\right]} \tag{B.9}$$

Equation (B.9) states that the amount of light that will remain trapped and propagate in the core is directly proportional to the square root of the product of the core refractive index and the core cladding refractive index difference.

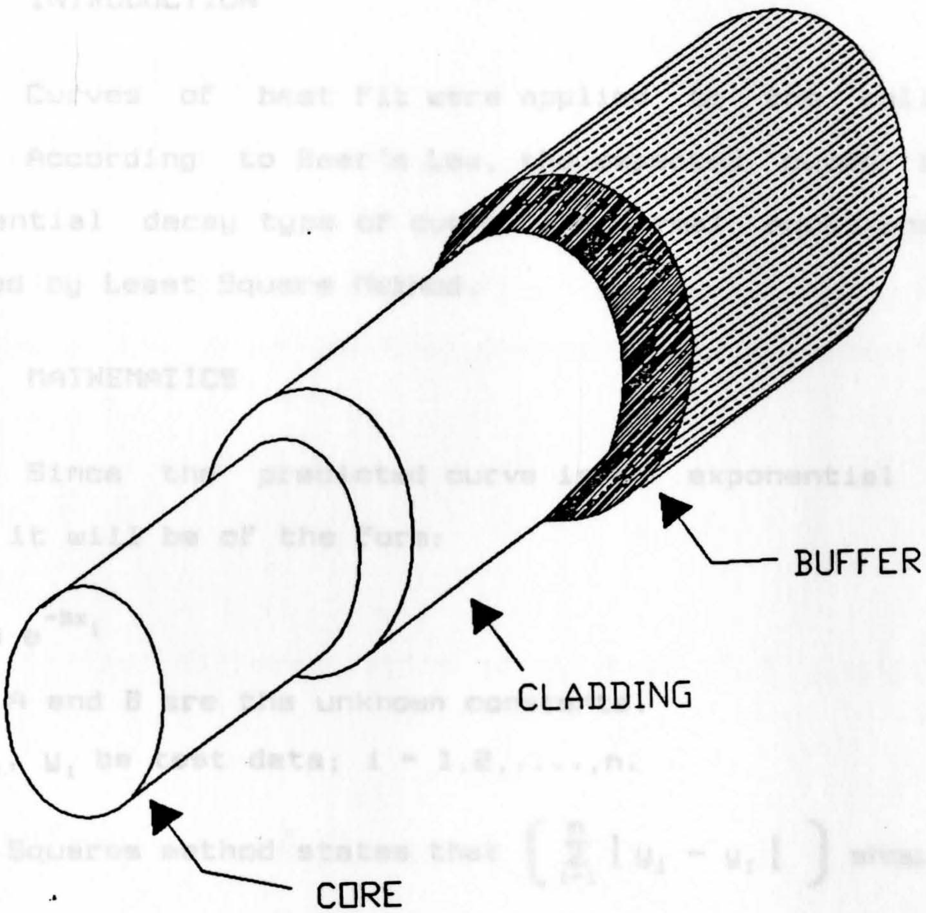

Fig. B.5 Cut-away view of an optical fiber (front end)

APPENDIX C

MATHEMATICS & DATA ANALYSIS

C.1 INTRODUCTION

Curves of best fit were applied to the collected data. According to Beer's Law, the expected curve is an exponential decay type of curve. The normal equations are derived by Least Square Method.

C.2 MATHEMATICS

Since the predicted curve is an exponential decay curve it will be of the form:

$$y_i = A\,e^{-Bx_i} \qquad \text{(C.1)}$$

where A and B are the unknown constants.

Let x_i, y_i be test data; $i = 1,2,\ldots,n$.

Least Squares method states that $\left(\sum_{i=1}^{n} | y_i - y_f | \right)$ should be a minimum where, y_i and y_f are the test data and fit, respectively.

Taking the natural logarithm of equation (C.1), we have,

$$\ln y_i = \ln A - B \cdot x_i \qquad \text{(C.2)}$$

Setting, $\ln y_i = \tilde{Y}_i$, $\ln A = \tilde{A}$ and $B = -\tilde{B}$, equation (C.2) can be written as,

$$\tilde{Y}_i = \tilde{A} + \tilde{B}\cdot x_i \tag{C.3}$$

Then the sum of the squares of the residuals is

$$I = \Sigma\left(Y_i - \tilde{Y}_i\right)^2 = \Sigma\left(\tilde{Y}_i - (\tilde{A} + \tilde{B}x_i)\right)^2 \tag{C.4}$$

where $I(\tilde{A},\tilde{B})$ and, $\tilde{A}$ and $\tilde{B}$ are unknown.

The objective now is to find $\tilde{A}$ and $\tilde{B}$ for the best exponential fit. This requires (necessary condition) that:

$$\left\{\begin{matrix} \dfrac{\partial I}{\partial \tilde{A}} = 0 \\ \dfrac{\partial I}{\partial \tilde{B}} = 0 \end{matrix}\right\}$$

Partial differentiation of equation (C.4) yields:

$$\frac{\partial I}{\partial \tilde{A}} = 2\Sigma\left[(\tilde{Y}_i - \tilde{A} - \tilde{B}\ x_i)(-1)\right] \tag{C.5}$$

$$\frac{\partial I}{\partial \tilde{B}} = 2\Sigma\left[(\tilde{Y}_i - \tilde{A} - \tilde{B}\ x_i)\ (-x_i)\right] \tag{C.6}$$

Equating equations (C.5) and (C.6) to zero produces the associated normal equations, that is,

$$\tilde{A}\cdot n + \tilde{B}\cdot\Sigma x_i = \Sigma\tilde{Y}_i \tag{C.7}$$

$$\tilde{A}\cdot\Sigma x_i + \tilde{B}\cdot\Sigma\left(x^2_i\right) = \Sigma(x_i\cdot\tilde{Y}_i) \tag{C.8}$$

where,

i = index ; i = 1, 2, 3, 4

n = 4

x_i = center-to-center distance from the transmitting OF to the receiving OF, in microns.

y_i = voltage in mV

$\sum(x_i)$ = the sum of all distances.

$\tilde{Y}_i = \ln y_i$

$\sum\tilde{Y}_i$ = the sum of data at respective distances in mV.

$\sum(x_i^2)$ = the sum of the squared distances.

Above parameters were calculated using Lotus 123™. Tables C.1 to C.5 give values of above parameters.

Table C.1

100% Coal Dust + 0% Rock Dust

i	x_i	y_i	x_i^2	$\tilde{Y}_i = \ln y_i$	$x_i\tilde{Y}_i$
1	1000	95	1×10^6	4.5539	4.554×10^3
2	1250	60	1.5625×10^6	4.0943	5.118×10^3
3	1500	22	2.25×10^6	3.0910	4.637×10^3
4	1750	4	3.0625×10^6	1.3863	2.426×10^3

From Table C.1 we have,

$$n = 4$$

$$\Sigma(x_i) = 5.5\times10^3$$

$$\Sigma(x_i^2) = 7.875\times10^6$$

$$\Sigma(\tilde{Y}_i) = 13.1255$$

$$\Sigma(x_i \cdot \tilde{Y}_i) = 16.735\times10^3$$

Substituting these values in simultaneous equations C.7 and C.8, and solving for A and B we obtain,

$A = 8602.8$ or $A \approx 8600$, $B = 4.2025\times10^{-3}$ or $B \approx 4.2\times10^{-3}$

Therefore, for 100% Coal Dust, the fitted curve is

$$y = 8600\ e^{-4.2\cdot10^{-3}x} \tag{C.9}$$

Table C.2
75% Coal Dust + 25% Rock Dust

i	x_i	y_i	x_i^2	$\tilde{Y}_i = \ln y_i$	$x_i\tilde{Y}_i$
1	1000	1400	1×10^6	7.2442	7.244×10^3
2	2000	400	4×10^6	5.9915	11.983×10^3
3	3000	100	9×10^6	4.6052	13.816×10^3
4	4000	30	16×10^6	3.4012	13.605×10^3

From Table C.2 we have,

$$n = 4$$

$$\Sigma(x_i) = 10\times10^3$$

$$\Sigma\left(x_i^2\right) = 30\times10^6$$

$$\Sigma\left(\tilde{Y}_i\right) = 21.2421$$

$$\Sigma\left(x_i\cdot\tilde{Y}_i\right) = 46.648\times10^3$$

Substituting these values in simultaneous equations C.7 and C.8, and solving for A and B we obtain,

$A = 5110.2$ or $A \approx 5100$, $B = 1.2914\times10^{-3}$ or $B \approx 1.29\times10^{-3}$

Therefore, for 75% Coal Dust + 25% Rock Dust the fitted curve is,

$$y = 5100\ e^{-1.29\cdot10^{-3}x} \qquad \text{(C.10)}$$

Table C.3

50% Coal Dust + 50% Rock Dust

i	x_i	y_i	x_i^2	$\tilde{Y}_i = \ln y_i$	$x_i\tilde{Y}_i$
1	1000	1680	1×10^6	7.4265	7.427×10^3
2	2000	600	4×10^6	6.3969	12.794×10^3
3	3000	140	9×10^6	4.9416	14.825×10^3
4	4000	20	16×10^6	2.9957	11.983×10^3

From Table C.3 we have,

$$n = 4$$
$$\Sigma(x_i) = 10\times10^3$$
$$\Sigma(x_i^2) = 30\times10^6$$
$$\Sigma(\tilde{Y}_i) = 21.7607$$
$$\Sigma(x_i\cdot\tilde{Y}_i) = 47.029\times10^3$$

Substituting these values in simultaneous equations C.7 and C.8, and solving for A and B we obtain,

$A = 9196.5$ or $A \approx 9200$, $B = 1.4746\times10^{-3}$ or $B \approx 1.47\times10^{-3}$

Therefore, for 50% Coal Dust + 50% Rock Dust the fitted curve is,

$$y = 9200\ e^{-1.47\cdot10^{-3}x} \tag{C.11}$$

Table C.4

25% Coal Dust + 75% Rock Dust

i	x_i	y_i	x_i^2	$\tilde{Y}_i = \ln y_i$	$x_i\tilde{Y}_i$
1	1000	4680	1×10^6	8.4511	8.451×10^3
2	2000	1720	4×10^6	7.4501	14.900×10^3
3	3000	560	9×10^6	6.3279	18.984×10^3
4	4000	140	16×10^6	4.9416	11.983×10^3

From Table C.4 we have,

$$n = 4$$

$$\Sigma(x_i) = 10\times10^3$$

$$\Sigma\left(x_i^2\right) = 30\times10^6$$

$$\Sigma\left(\tilde{Y}_i\right) = 27.1707$$

$$\Sigma\left(x_i\cdot\tilde{Y}_i\right) = 62.101\times10^3$$

Substituting these values in simultaneous equations C.7 and C.8, and solving for A and B we obtain,

$A = 16408$ or $A \approx 16400$, $B = 1.1652\times10^{-3}$ or $B \approx 1.17\times10^{-3}$

Therefore, for 25% Coal Dust + 75% Rock Dust the fitted curve is

$$y = 16400\ e^{-1.17\cdot10^{-3}x} \qquad (C.12)$$

Table C.5

0% Coal Dust + 100% Rock Dust

i	x_i	y_i	x_i^2	$\tilde{Y}_i = \ln y_i$	$x_i\tilde{Y}_i$
1	1000	14500	1×10^6	9.582	9.582×10^3
2	2000	2500	4×10^6	7.824	15.648×10^3
3	3000	800	9×10^6	6.685	20.055×10^3
4	4000	300	16×10^6	5.704	22.816×10^3

From Table C.5 we have,

$$n = 4$$

$$\Sigma(x_i) = 10\times10^3$$

$$\Sigma(x_i^2) = 30\times10^6$$

$$\Sigma(\tilde{Y}_i) = 29.795$$

$$\Sigma(x_i\cdot\tilde{Y}_i) = 68.101\times10^3$$

Substituting these values in simultaneous equations C.7 and C.8, and solving for A and B we obtain,

$A = 41858.5$ or $A \approx 41900$, $B = 1.2773\times10^{-3}$ or $B \approx 1.28\times10^{-3}$

Therefore, for 0% Coal Dust + 100% Rock Dust the fitted curve is,

$$y = 41900\ e^{-1.28\cdot10^{-3}x} \qquad (C.13)$$

Setting $y = F$ and $x = d$ in normal equations C.7 and C.8. Whereas, constants are $A(F_o, \alpha_s$ and $\Delta)$ and $B(\alpha_s)$.

Finally, actual constants to be found are α_t, α_s and α_r.

Various normal exponential fits derived are plotted (see figures C.1 to C.5), using MathCAD™

Data collected show a monotonic behavior and are recorded in Table C.6 for various percentages of RD concentration in the sample.

TABLE C.6

Monotonic behavior of the data (all in mV).

Distance µm	% Rock Dust in sample				
	100	75	50	25	0
1000	14500	4800	1650	1350	95
2000	2500	1720	600	410	2
3000	850	560	150	100	0
4000	300	150	50	40	0

$N := 4000$ $\qquad\qquad$ $x := 0, 1 \,..N$

$$y(x) := 8600 \cdot e^{-\left[4.20 \cdot 10^{-3} \cdot x\right]}$$

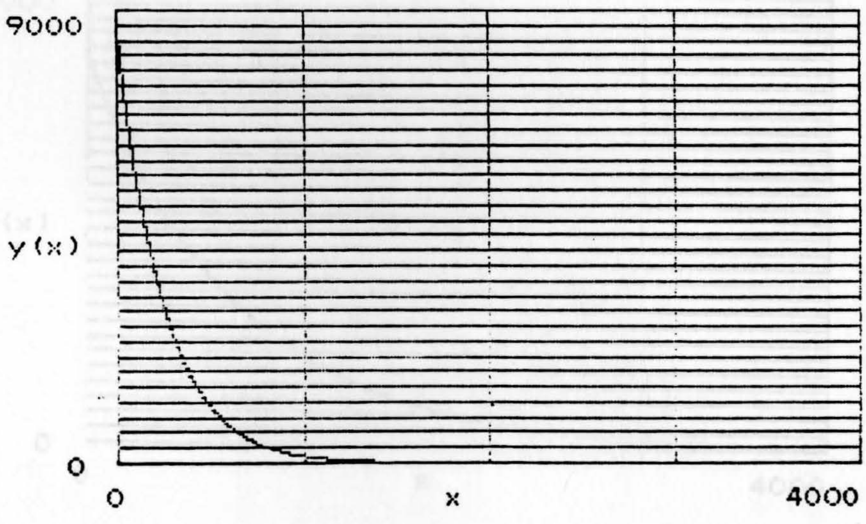

Fig. C.1 Fitted curve for 100% Coal Dust

$N := 4000 \qquad x := 0, 1 \,..\, N$

$y(x) := 5100 \cdot e^{-\left[1.29 \cdot 10^{-3} \cdot x\right]}$

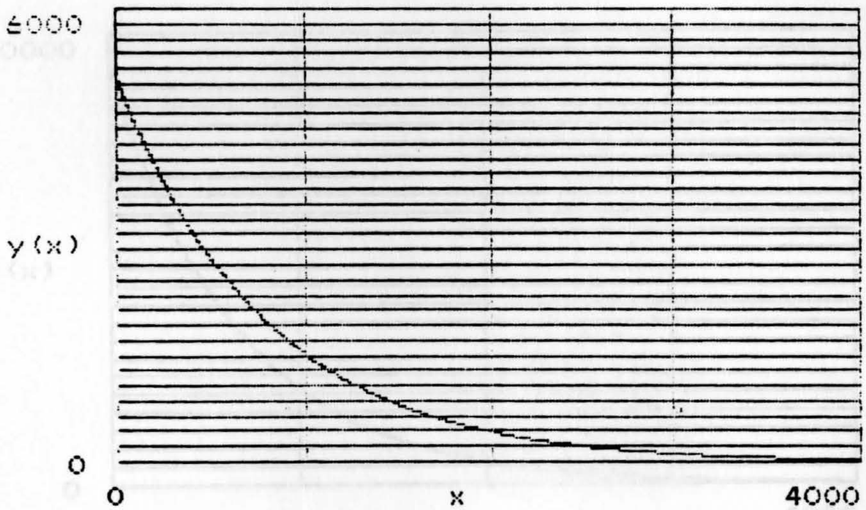

Fig. C.2 Fitted curve for 75% Coal Dust and 25% Rock Dust.

$N := 4000$ $\qquad$ $x := 0, 1 .. N$

$$y(x) := 9200 \cdot e^{-\left[1.47 \cdot 10^{-3} \cdot x\right]}$$

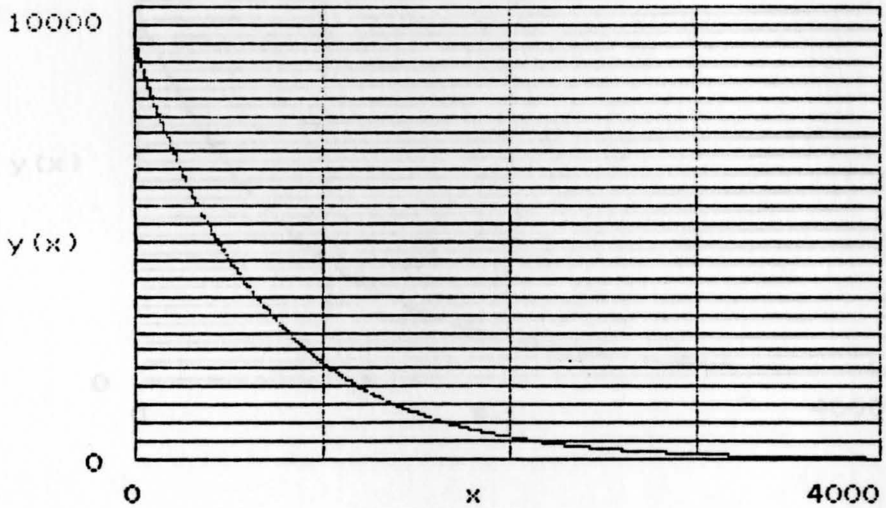

Fig. C.3 Fitted curve for 50% Coal Dust and 50% Rock Dust.

$N := 4000 \qquad x := 0, 1 \,..\, N$

$$y(x) := 16400 \cdot e^{-\left[1.17 \cdot 10^{-3} \cdot x\right]}$$

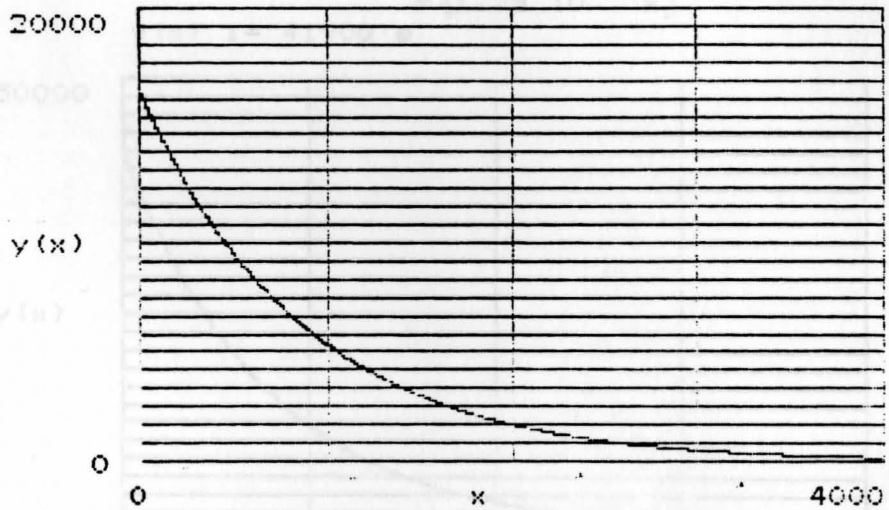

Fig. C.4 Fitted curve for 25% Coal Dust and 75% Rock Dust.

$N := 4000 \qquad x := 0,1\,..N$

$$y(x) := 41900 \cdot e^{-\left[1.28 \cdot 10^{-3} \cdot x\right]}$$

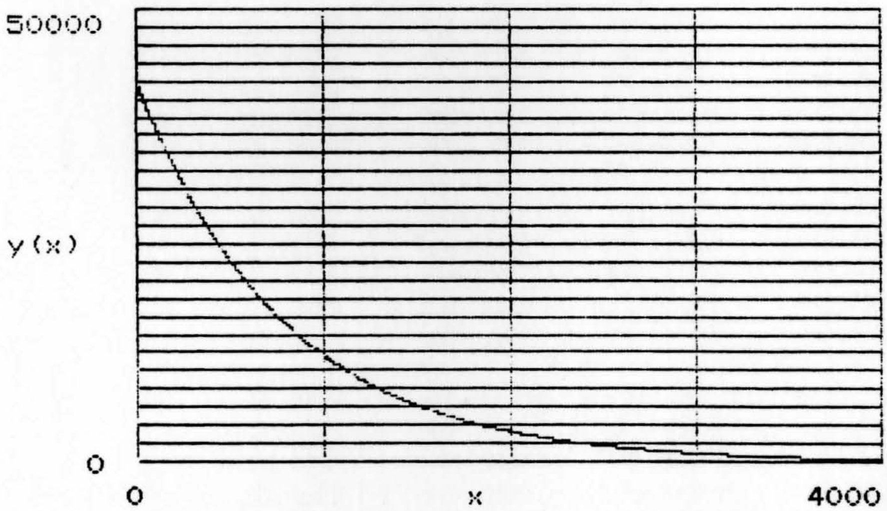

Fig. C.5 Fitted curve for 100% Rock Dust.

APPENDIX D

EXPERIMENTAL DATA TABLES

All the test data obtained during the experiment are given in Tables D.1 to D.5.

TABLE D.1

100% COAL DUST + 0% ROCK DUST

All measurements in Volts

	1000 µm	2000 µm	3000 µm	4000 µm
01	0.045	-0.012	-0.025	-0.028
02	0.047	-0.013	-0.024	-0.027
03	0.045	-0.014	-0.024	-0.026
04	0.058	-0.011	-0.023	-0.025
05	0.045	-0.011	-0.022	-0.025
06	0.046	-0.018	-0.023	-0.023
07	0.043	-0.017	-0.012	-0.013
08	0.037	-0.008	-0.011	-0.013
09	0.078	-0.008	-0.026	-0.029*
10	0.092	-0.009	-0.024	-0.013
11	0.088	-0.008	-0.024	-0.027
12	0.087	-0.002	-0.024	-0.028
13	0.082	-0.007	-0.024	-0.028
14	0.089	-0.005	-0.025	-0.028
15	0.087	-0.000	-0.023	-0.027
16	0.089	-0.008	-0.025	-0.028
17	0.098	-0.013	-0.026	-0.029*
18	0.103	-0.016	-0.026	-0.029
19	0.088	-0.015	-0.026	-0.029
20	0.081	-0.016	-0.026	-0.029
21	0.088	-0.003	-0.024	-0.028
22	0.112	-0.007	-0.022	-0.027
23	0.103	-0.008	-0.021	-0.026
24	0.123	-0.004	-0.022	-0.027
25	0.121	-0.007	-0.022	-0.027
26	0.110	-0.006	-0.022	-0.027
27	0.091	-0.002	-0.023	-0.027
28	0.119	-0.011	-0.019	-0.025
29	0.120	-0.007	-0.020	-0.026
30	0.109	-0.005	-0.021	-0.025

* Cleaned fiber tips in the probe

TABLE D.2

75% COAL DUST + 25% ROCK DUST

All measurements in Volts

	1000 μm	2000 μm	3000 μm	4000 μm
01	1.340	0.395	0.109	0.033
02	1.740	0.260	0.020	0.025
03	1.410	0.312	0.022	0.027
04	1.370	0.555	0.142	0.040
05	1.320	0.586	0.133	0.037
06	1.700	0.264	0.070	0.027
07	1.460	0.455	0.101	0.035
08	1.440	0.122	0.039	0.027
09	1.470	0.482	0.108	0.039
10	1.680	0.469	0.115	0.033
11	1.520	0.366	0.089	0.028
12	1.280	0.465	0.131	0.036
13	1.520	0.402	0.103	0.029
14	1.540	0.273	0.067	0.023
15	1.160	0.344	0.088	0.032
16	1.350	0.321	0.070	0.027
17	1.270	0.378	0.091	0.031
18	1.490	0.365	0.079	0.029
19	1.500	0.199	0.053	0.025
20	1.180	0.554	0.168	0.038

Ratio by weight - 12 gms Coal Dust
4 gms Rock Dust

TABLE D.3

50% COAL DUST + 50% ROCK DUST

All measurements in Volts

	1000 μm	2000 μm	3000 μm	4000 μm
01	3.280	0.568	0.095	0.022
02	1.780	0.445	0.090	0.028
03	1.650	0.543	0.113	0.023
04	1.630	0.605	0.135	0.035
05	1.480	0.641	0.147	0.040
06	1.530	0.568	0.120	0.025
07	1.570	0.615	0.085	0.021
08	1.560	0.511	0.107	0.038
09	1.590	0.452	0.092	0.026
10	2.000	0.790	0.179	0.048
11	1.950	0.678	0.208	0.031
12	1.520	0.535	0.133	0.033
13	1.340	0.533	0.135	0.029
14	1.290	0.535	0.113	0.021
15	2.230	0.770	0.057	- 0.005
16	3.300	0.740	0.199	0.043
17	3.580	1.035	0.237	0.041
18	2.850	0.458	0.125	0.025
19	3.120	1.090	0.235	0.048
20	2.960	0.650	0.145	0.033

Ratio by weight - 8 gms Coal Dust
8 gms Rock Dust

No light 12 mV to 16 mV

TABLE D.4

25% COAL DUST + 75% ROCK DUST

All measurements in Volts

	1000 µm	2000 µm	3000 µm	4000 µm
01	5.850	2.100	0.592	0.130
02	4.950	1.860	0.486	0.096
03	3.220	1.780	0.778	0.175
04	3.980	2.020	0.747	0.160
05	5.050	1.910	0.525	0.108
06	3.930	1.790	0.565	0.118
07	4.210	1.830	0.591	0.120
08	3.990	1.930	0.709	0.155
09	5.310	1.720	0.455	0.100
10	4.860	1.630	0.420	0.088
11	4.850	1.730	0.489	0.087
12	4.870	1.810	0.535	0.087
13	4.140	1.830	0.650	0.124
14	4.290	1.820	0.563	0.114
15	4.610	1.690	0.542	0.116
16	4.140	1.780	0.598	0.117
17	4.260	1.810	0.563	0.103
18	4.350	1.740	0.525	0.092
19	4.010	1.690	0.546	0.102
20	4.460	1.650	0.467	0.084

Ratio by weight - 4 gms Coal Dust
12 gms Rock Dust

TABLE D.5

0% COAL DUST + 100% ROCK DUST

All measurements in Volts

	1000 µm	2000 µm	3000 µm	4000 µm
01	14.60	2.600	0.666	0.289
02	13.30	3.300	0.990	0.385
03	11.60	2.300	0.745	0.222
04	14.60	1.760	0.725	0.316
05	11.80	1.580	0.737	0.336
06	13.60	1.600	0.197	0.149
07	14.80	1.670	0.178	0.164
08	14.80	2.500	0.954	0.434*
09	14.80	2.040	0.920	0.430
10	14.50	2.090	0.845	0.374
11	13.70	1.320	0.578	0.320
12	14.80	2.480	0.853	0.420
13	14.80	2.300	0.835	0.400
14	14.40	1.670	0.583	0.292
15	14.80	2.720	0.925	0.424
16	14.80	2.180	0.824	0.425
17	14.80	2.220	0.815	0.349
18	14.80	2.460	0.784	0.331
19	14.80	3.280	0.906	0.346
20	14.80	2.060	0.710	0.314

* After cleaning the fiber tips of the probe

APPENDIX E

EQUIPMENT AND DEVICES

LIGHT SOURCE:

He-Ne Laser, Wavelength 632.8 nm, 0.95 mW
Spectra-Physics Inc., California-94042.

OPTICAL FIBERS:

ESKAEXTRA™
Plastic Fiber, Type EH-4001,
Mitsubishi Rayon Co., Ltd.

FIBER CONNECTORS:

a. Single Position Plug Part No. 228087-1
b. Connector Kit, Part No. 530530-2
c. Active Device Mount, Part No. 530563-1

AMP Products, USA.

DIGITAL MULTIMETER:

DVM56 "MICRORANGER"
SENCORE, South Dakota.

POWER SUPPLY:

LPS-151/152 dc tracking Power Supply
Leader Instruments Corporation, New York.

BREADBOARD:

Specially designed at Electrical/Electronic Engineering Department, Kent State University, Trumbull Campus, Warren.

PROBE BLOCK:

Specially fabricated at the US Bureau of Mines Workshop, Pittsburgh, Pennsylvania.

APPENDIX F

LIST OF HARDWARE & SOFTWARE

HARDWARE

1. Computer - Samsung™ Model S550

2. Printer - Star Micronics™ SG10

SOFTWARE

3. Word-Processing - WORDSTAR™ Rel 5.5

   Wordstar USA.

4. Technical Word-Processing - EXACT™

   Technical Support Software Inc.,

5. Worksheet - LOTUS™ 1-2-3™ Student Ed.

   Lotus Development Corporation
   Published by Addison-Wesley

6. CAD - AUTOCAD™ Rel 9*

   Autodesk, Inc.

   - MathCAD™ Ver. 2.0 Student Edition.

   MathSoft Inc., published by Addison-Wesley Publishing Company, Inc.,& Benjamin/Cummings Publishing Company, Inc.

7. Overhead Transparencies - KGS™ *

   Kinematic Graphics

*(courtesy of Kent State University, Trumbull Campus)

BIBLIOGRAPHY

1. U.S. Code of Federal Regulations. Title 30-Mineral Resources; Chapter I - Mine Safety and Health Administration, Department of Labor; Subpart E - Combustible Materials and Rock Dusting; Part 75.402 - Rock Dust; July 1, 1985.

2. Perlee, Henry E., Pinkerton, John E., and Sapko, Michael J., "Optical Rock Dust Meter - Part I", unpublished.

3. Bonner, R.F., et al., "Model for Photon Migration in Turbid Biological Media", Optical Society of America, Vol. 4, No. 3, March 1987.

4. Coleman, J. Todd, et al., "Fiber Optic Based Sensor for Bioanalytical Absorbance Measurements", Anal. Chem., Vol. 56, pp 2249-51, 1984.

5. Johnson, Curtis C., "Optical Diffusion in Blood" IEEE Trans. on Bio-Medical Engineering, Vol. BME-17, No.2, April 1970.

6. Johnson, Curtis C., "Nonionizing Electromagnetic Wave Effects in Biological Materials and Systems" Proceedings of IEEE, Vol. 60, No. 6, June 1972.

7. Peterson, John I. and Vurek, Gerald G., "Fiber-Optic Sensors for Biomedical Applications" Science, Vol. 224, pp 123-7, April-June 1984.

8. Reynolds, Larry, et al., "Diffuse Reflectance from a Finite Blood Medium: Applications to the Modeling of Fiber Optic Catheters", Applied Optics, Vol. 15, No. 9, September 1978.

9. W., M.D., "Bioanalytical Applications of Fiber-Optic Chemical Sensors" Analytical Chemistry, Vol. 58, No. 7, June 1986.

10. Zdrojkowski, R.J., and Pisharoty, N.R., "Optical Transmission and Reflection by Blood" IEEE Transactions on Bio-Medical Engineering, Vol. BME-17, No. 2, April 1970.

12. Meiksin, Z.H., and Thackray, Philip C., Electronic Design with Off-the-Shelf Integrated Circuits, Parker Publishing Co., 1982.

13. Sze, S.M., Physics of Semiconductor Devices, A Wiley-Interscience Publication, 2nd ed., 1981.

REFERENCES

BOOKS

Allocca, John A. and Stuart, Allen, Transducers Theory & Applications, Reston Publishing Company, Inc., 1984.

Cheo, Peter K., Fiber Optics Devices and Systems, Prentice-Hall, Inc., 1985.

Cherin, Allen H., An Introduction to Optical Fibers, McGraw-Hill Book Company, 1983.

Davis, Charles M., et al., Fiberoptic Sensor Technology Handbook, Optical Technologies, Inc., 1986.

Forbes, Mark, Writing Technical Articles, Speech, and Manuals, John Wiley & Sons, 1988.

Hecht, Jeff, Understanding Fiber Optics, Howard W. Sams & Company, 1987.

Hentschel, Christian, Fiber Optics Handbook, Hewlett-Packard GmbH, 1988.

Holman, J.P., Experimental Methods for Engineers, McGraw-Hill Book Company, 1989, 5e.

Ishimaru, Akira, Wave Propagation and Scattering in Random Media, Vol. I, Academic Press, Inc., 1978.

Jeunhomme, Luc B., Single-Mode Fiber Optics Principles and Applications, Marcel Dekker, Inc., 1983.

Johnson, Curtis D., Process Instrumentation Technology, John Wiley & Sons, 1988, 3e.

Jones, Kenneth A., Introduction to Optical Electronics, Harper & Row Publishers, 1987.

Kahaner, D., Moler, C., and Nash, S., Numerical Methods and Software, Prentice-Hall, Inc. 1989.

Kao, Charles K., Optical Fiber Systems Technology, Design and Applications, McGraw-Hill Book Company, 1982.

Kennedy, E.J., Operational Amplifier Circuits - Theory and Applications, Holt, Rinehart and Winston, Inc., 1988.

Meiksin, Z.H., and Thackray, P.C., Electronic Design with Off-the-Shelf Integrated Circuits, Parker Publishing Company, Inc., 1982.

Money, S.A., Microprocessors in Instrumentation and Control, McGraw-Hill Book Company, 1985.

Monograph ,Directions for Format and Presentation of a Master's Thesis, The Graduate School, Youngstown State University, April 1970.

Nérou, Jean Pierre Introduction to Fiber Optics, Les Editions Le Griffon D'Argile Inc., Quebéc, Canada, 1988.

Ramo, Simon, et al., Fields and Waves in Communication Electronics, John Wiley & Sons, 1984, 2e.

Scheid, Francis Numerical Analysis, Schaum's Series, McGraw-Hill Book Company, 1988, 2 ed.

Spiegel, Murray R., Advance Calculus, Schaum's Outline Series, McGraw-Hill Book Company, 1963.

Spiegel, Murray R., Advanced Mathematics, Schaum's Outline Series, McGraw-Hill Book Company, 1971.

Spiegel, Murray R., Vector Analysis, Schaum's Outline Series, McGraw-Hill Book Company, 1959.

Sterling, Jr., Donald J., Technician's Guide to Fiber Optics, Delmar Publishers Inc., 1987.

Tischler, Morris, Opto-electronics A Text-Lab Manual, McGraw-Hill Book Company, 1986.

Wolf, Helmut F., editor, Handbook of Fiber Optics: Theory and Applications, Garland STPM Press, 1979.

ARTICLES

Altmann, K., "Space-time Distortion of Laser Pulses due to Multiple Scattering in Particulate Media", Applied Optics, Vol. 27, No. 12, pp 2451 - 60, June 15, 1988.

Beheim, Glen and Anthan, Donald J., "Loss-Compensation of Intensity-Modulating Fiber-Optic Sensors", NASA Technical Memorandum 88825, September 1986.

Berthold, J.W., "Overview of Fiber-Optic Intensity Sensors for Industry", SPIE Vol. 838 Fiber Optic and Laser Sensors V, 1987.

Black, Richard J., and Ankiewicz, Adrian, "Fiber-optic Analogies with Mechanics", Am. J. Phys, 53(6), June 1985.

Bonner, R.F., et al., "Model for Photon Migration in Turbid Biological Media", Optical Society of America, Vol. 4, No. 3, March 1987.

Boyle, W.S., "Light-Wave Communications", Scientific American, Vol. 237 No. 2, August 1987.

Brignell, J.E., " Digital Compensation of Sensors", IOP Publishing Ltd., 1987, pp 1097 - 1102.

Coleman, J. Todd, et al., "Fiber Optic Based Sensor for Bioanalytical Absorbance Measurements", Anal. Chem., Vol. 56, pp 2249-51, 1984.

Conley, Michael P., et al., "Reflection Type Fiber-Optic Sensor", SPIE, Vol. 718 Fiber Optic and Laser Sensors IV, 1986, pp 237-243.

Dandridge, A., and Miles, R.O., "Fiber Optic Sensors", CEP, January 1986.

DePaula, R.P. and Moore, E.L., "Overview of Fiber-Optical Sensors", NASA Tech. Brief, Vol. 11, No. 7, Item# 84, August 1987.

Fairaizl, Alan F., "How to Select Fiber Optic Cables for Practical Applications", Siecor Optical Cables, Inc.

Gambling, W.A., "Novel Optical Fibers for Sensing Applications", Journal of Physics & Electronics, U.K., Vol. 20, No. 9, September 1987.

Giallorenzi, Thomas G., et al., "Optical Fiber Sensor Technology", IEEE Journal of Quantum Electronics, Vol.QE-18, No. 4, April 1982.

Gilliar, Wolfgang, et al., "Light Scattering from Fibers : An Extension of a Single-slit Diffraction Experiment", Am. J. Phys, 55(6), June 1987.

Gloge, D., "Weakly Guiding Fibers", Applied Optics, Vol. 10, No. 10, October 1971.

Groenhuis, R.A.J., et al., "Scattering and Absorption of Turbid Materials Determined from Reflection Measurements. 1: Theory", Applied Optics, Vol. 22, No. 16, August 15, 1983.

Groenhuis, R.A.J., et al., "Scattering and Absorption of Turbid Materials Determined from Reflection Measurements. 2: Measuring Method and Calibration", Applied Optics, Vol. 22, No. 16, August 15, 1983.

Haltrin, Vladimir I., "Exact Solution of the Characteristic Equation for Transfer in the Anisotropically Scattering and Absorbing Medium", Applied Optics, Vol. 27, No. 3, February 1, 1988.

Hanse, Joel G., "Linearized Fiber Optic Sensor Readout" Optical Engineering", Vol. 23, No. 3, May/June 1984.

Ishimaru, Akira, "Theory and Application of Wave Propagation and Scattering in Random Media", Proceedings of IEEE, Vol. 65, No. 7, July 1977.

Jackson, D.A., and Jones, J.D.C., "Fiber Optic Sensors", Optica Acta, Vol. 33, No. 12, 1986.

Johnson, Curtis C., "Optical Diffusion in Blood" IEEE Trans. on Bio-Medical Engineering, Vol. BME-17, No. 2, April 1970.

Johnson, Curtis C., "Nonionizing Electromagnetic Wave Effects in Biological Materials and Systems" Proceedings of IEEE, Vol. 60, No. 6, June 1972.

Jordan, G.R., " Sensor Technologies of the Future", GEC Review", Vol. 3, No. 1, 1987.

Keijer, Marleen, et al.,"Optical Diffusion in Layered Media", Applied Optics, Vol. 27, No. 9, May 1, 1988.

Kubelka, Paul "New Contributions to the Optics of Intensely Light-Scattering Materials. Part I" Journal of the Optical Society of America, Vol. 38, No. 5, May 1948.

Kubelka, Paul "New Contributions to the Optics of Intensely Light-Scattering Materials. Part II: Nonhomogeneous Layers" Journal of the Optical Society of America, Vol. 44, No. 4, April 1954.

Latimer, Paul and Noh, Seung Jeong " Light Propagation in Moderately Dense Particle Systems: A Reexamination of the Kubelka- Munk Theory" Applied Optics, Vol. 26, No. 3, February 1, 1987.

Ma, Yushieh, et al., "Scattered Intensity of a Wave Propagating in a Discrete Random Media" Applied Optics, Vol. 27, No. 12, June 15, 1988.

Maheu, B. and Gouesbet, G., "Four-flux Models to solve the Scattering Transfer Equation: Special Cases", Applied Optics, Vol. 25, No. 7, April 1, 1986.

Maheu, B. et al., "Four-flux Models to solve the Scattering Transfer Equation in terms of Lorenz- Mie Parameters", Applied Optics, Vol. 23, No. 19, October 1, 1984.

McMahon, Donald H., et al., "Fiber-Optic Transducers", IEEE Spectrum, December 1981.

Mudgett, P.S. and Richards, L.W., "Multiple Scatter Calculations for Technology" Applied Optics, Vol. 10, No. 7, July 1971.

Murphy, Kevin W., "Fiber Myths Debunked", Network World, January, 1987, pp 41 - 43.

Nossal, Ralph, et al., "Photon Migration in Layered Media" Applied Optics, Applied Optics, Vol. 27, No. 16, August 15, 1988.

Peterson, John I. and Vurek, Gerald G., "Fiber-Optic Sensors for Biomedical Applications" Science, Vol. 224, pp 123-7, April-June 1984.

Ohr, Stephan "Fiber-Optic Semis Carve Out Wider Infrared Territory", Electronic Design 2, January 1980.

Reynolds, Larry, et al., "Diffuse Reflectance from a Finite Blood Medium: Applications to the Modeling of Fiber Optic Catheters", Applied Optics, Vol. 15, No. 9, September 1978.

Seitz, W. Rudolf "Chemical Sensors Based on Fiber Optics" Analytical Chemistry, Vol. 56, No. 1, January 1984.

Spillman Jr., W.B., "Industrial uses of Fiber Optic Sensors", SPIE, Vol. 718 Fiber Optic and Laser Sensors IV, 1986.

Thomsen, Dietrick E., "Optical Fiber Sensors: Just Around the Corner" Science News, Vol. 127, April 6,1985.

Tsang, Leung and Ishimaru, Akira "Theory of Backscattering Enhancement of Random Discrete Isotropic Scatterers Based on the Summation of all Ladder and Cyclical Terms" Optical Society of America, Vol. 2, No. 8, August 1985.

W., M.D., "Bioanalytical Applications of Fiber-Optic Chemical Sensors" Analytical Chemistry, Vol. 58, No. 7, June 1986.

White, Richard M., "A Sensor Classification Scheme", IEEE Transaction on Ultrasonic, Ferroelectrics, and Frequency Control, Vol. UFFC-34, No. 2, March 1987.

Zdrojkowski, R.J., and Pisharoty, N.R., "Optical Transmission and Reflection by Blood" IEEE Transactions on Bio-Medical Engineering, Vol. BME-17, No. 2, April 1970.

SEMINAR PROCEEDINGS

Crome, Edward F., "Introduction to Fiber Optic Sensors", Proceedings of the Seminar at John Carrol University, Cleveland, Ohio, October, 1988.

PRODUCT CATALOGS

AMPHENOL:

Fiber Optic Products Catalog.

CORNING GLASS WORKS - Telecommunications Products Divn.:

Product Information :
1. Flexcore Specialized Single-Mode Fiber
2. Flexcore-850 Single-Mode Fiber
3. 50/125 μm LDF CPC3 Multimode Optical Fiber
4. 62/125 μm CPC3 Multimode Optical Fiber
5. 85/125 μm CPC3 Multimode Optical Fiber
6. 100/140 μm CPC2 Multimode Optical Fiber
7. PI-112 Polarization-Retaining Single-Mode Fiber, 6/86
8. PI-113 Corshield Hermetic Coating for Corguide Fibers
9. PRSM Polarization-Retaining Single Mode Fiber
10. SMF-21 CPC3 Single-Mode Optical Fiber
11. SMF-28 CPC3 Single-Mode Optical Fiber
12. SMF/DS CPC3 Single-Mode Dispersion-Shifted Optical Fibers

"GuideLines", Vol. 1, No. 3, 1985.
Vol. 2, No. 2, and 3, 1986.
Vol. 3, Nos. 1,2,3, and 4, 1987.

EOTec Corporation:

"Industrial Fiber Optic Communication Links and Sensors", A Complete Reference Manual & Product Catalog.

"Fiber Optic Sensors", A Complete Reference Manual & Product Catalog.

Hewlett-Packard

Led Indicators and Displays Applications Handbook, 1986.

Optocouplers and Fiber Optics Applications Handbook, 1986.

Optoelectronics Designer's Catalog, 1988 - 1989.

Mitsubishi Rayon Co., Ltd.

ESKA Cables, Technical Bullitin.

Motorola

Optoelectronics Device Data, 1988.